死を起こすので原則行わない.

維持治療：吸入投与，1ヵ月に1回，300mgを蒸留水に溶解し，30分程度の吸入時間となるように希釈量を調整して吸入投与．この吸入投与は軽症の初期治療としても用いることができる．この場合は1日1回吸入する.

3)初期治療には用いられない．1)，2)が使用できない場合に維持治療(発症予防)に用いられることがある.

主作用

1)合剤のいずれの薬剤も葉酸代謝経路の阻害剤で，ニューモシスチスの葉酸合成を阻害することで活性を発揮する.

2)ニューモシスチスのグルコース代謝および蛋白質合成を抑制するとされるが，正確な作用機序は明らかでない.

副作用と対策

1)本剤の重要な副作用としてはアレルギー反応で，とくにHIV感染者では頻度が高い．投与開始直後のStevens-Johnson症候群や中毒性表皮壊死症(TEN)，投与開始後5～14日頃に見られる発熱，発疹などに注意を払い，発症した場合にはすみやかに中止する．また，骨髄障害も頻度が高く白血球減少，貧血などがみられる．電解質異常(高K血症，低Na血症)も頻度が高い．本剤による腎機能障害も見られる.

2)重要な副作用は腎機能障害，膵炎，低血糖，があげられる．また投与速度が速いと低血圧やショック様症状を呈するため，添付文書に示される時間よりは長い時間をかけて(2～3時間)投与する方が安全である．このほか電解質異常や味覚異常，口唇や四肢の知覚異常の頻度も高い．本剤投与による意識障害や錯乱，骨髄障害を見ることもある．副作用を早期に発見するために本剤投与中は週2回以上の血液検査を行うとともに，自覚症状の出現に注意を払う必要がある.

3)過敏症症状，骨髄障害が見られることがある.

禁忌

1)妊婦または妊娠している可能性のある女性，低出生体重児，新生児，グルコース-6-リン酸脱水素酵素(G-6-PD)欠乏患者，本剤の成分またはサルファ剤に対し過敏症の既往歴のある患者.

2)ザルシタビン・ホスカルネットを投与中の患者，本剤に対する過敏症の既往歴のある患者.

吸入投与は，換気障害が重症の患者(PaO_2 60mmHg以下).

3)本剤に対する過敏症の既往歴のある患者.

解説

ニューモシスチス肺炎の治療は，効果発現の高さからST合剤が第1選択である．ST合剤はおもに過敏症と骨髄障害，ペンタミジンは腎機能障害や味覚障害や低血圧など，重篤な副作用の頻度が高く，使用にあたっては厳重な経過観察が必要である．一方の薬剤で副作用が見られた場合は，他方に切り替える．おおむね10日以上の治療が行われて改善が見られるものの，副作用などで両剤の投与が難しくなった場合には，ペンタミジンの吸入投与も用いることができる．ニューモシスチス肺炎の治療は21日間を原則とする.

ニューモシスチス肺炎治療では治療薬の投与とともに十分な副腎皮質ステロイドホルモンを開始して，治療に伴う過剰な炎症と，それによる肺の器質化を防止することが治療成功の鍵となる.

〈キーワード〉ノイラミニダーゼ　異常行動　骨髄障害　腎機能障害　吸入投与　副腎皮質ステロイドホルモン

研究成果の刊行に関する一覧表

平成 20 年度　国立感染症研究所　片野晴隆

雑誌

発表者氏名	論文タイトル名	発表誌名	巻号	ページ	出版年
Dewan, MZ, Takamatsu, N, Hidaka, T, Hatakeyama, K, Nakahata, S, Fujisawa, J, Katano, H, Yamamoto, N, Morishita, K.	Critical role for TSLC1 expression in the growth and organ infiltration of adult T-cell leukemia cells in vivo. J Virol.	J. Virol.	82	11958-11963	2008
Dewan, MZ, Tomita, M, Katano, H, Yamamoto, N, Ahmed, S, Yamamoto, M, Sata, T, Mori, N, Yamamoto, N.	An HIV protease inhibitor, ritonavir targets the nuclear factor-kappaB and inhibits the tumor growth and infiltration of EBV-positive lymphoblastoid B cells.	Int J Cancer.	124	622-629	2009

JOURNAL OF VIROLOGY, Dec. 2008, p. 11958–11963
0022-538X/08/$08.00+0 doi:10.1128/JVI.01149-08

Vol. 82, No. 23

NOTES

Critical Role for TSLC1 Expression in the Growth and Organ Infiltration of Adult T-Cell Leukemia Cells In Vivo▽

M. Zahidunnabi Dewan,[1,2]† Naofumi Takamatsu,[3] Tomonori Hidaka,[4] Kinta Hatakeyama,[5] Shingo Nakahata,[3] Jun-ichi Fujisawa,[6] Harutaka Katano,[7] Naoki Yamamoto,[1,2]* and Kazuhiro Morishita[3]*

Department of Molecular Virology, Graduate School, Tokyo Medical and Dental University, 1-5-45 Yushima, Bunkyo-ku, Tokyo 113-8519, Japan[1]; AIDS Research Center, National Institute of Infectious Disease, 1-23-1 Toyama, Shinjuku-ku, Tokyo 162-8640, Japan[2]; Department of Medical Sciences,[3] Department of Internal Medicine,[4] and Department of Pathology,[5] Faculty of Medicine, University of Miyazaki, Kiyotake, Miyazaki, Japan; Department of Microbiology, Kansai Medical University, Moriguchi, Osaka, Japan[6]; and Department of Pathology, National Institute of Infectious Diseases, 1-23-1 Toyama, Shinjuku-ku, Tokyo 162-8640, Japan[7]

Received 2 June 2008/Accepted 15 September 2008

Adult T-cell leukemia (ATL) is associated with human T-cell leukemia virus type 1 infection. The tumor suppressor lung cancer 1 (TSLC1) gene was previously identified as a novel cell surface marker for ATL, and this study demonstrated the involvement of TSLC1 expression in tumor growth and organ infiltration of ATL cells. In experiments using NOD/SCID/γc^{null} mice, both leukemia cell lines and primary ATL cells with high TSLC1 expression caused more tumor formation and aggressive infiltration of various organs of mice. Our results suggest that TSLC1 expression in ATL cells plays an important role in the growth and organ infiltration of ATL cells.

Human T-cell leukemia virus type 1 (HTLV-1) is the causative agent of an aggressive form of $CD4^+$ T-cell leukemia termed adult T-cell leukemia (ATL) (7, 14, 18). Carriers of HTLV-1 have been identified in a number of locations throughout the world, including parts of Africa; Papua New Guinea; specific regions in Europe including Romania; parts of South America including northern Brazil, Peru, northern Argentina, and Colombia; and the southern part of Kyushu in Japan (17). Common findings in patients with ATL include enlargement of peripheral lymph nodes, hepatomegaly, splenomegaly, skin infiltration, and hypercalcemia. The Tax gene is a unique viral gene thought to play a central role in HTLV-1-induced transformation. It is responsible for transactivation of the HTLV-1 long terminal repeat (5, 16) and numerous cellular genes involved in T-cell activation and growth, including those encoding interleukin-2 (IL-2) (11) and the α chain of IL-2 receptor (IL-2Rα) (CD25, Tac) (1, 2). The long latency of ATL development suggests that multiple genetic events accumulate in HTLV-1-infected cells; however, the precise molecular mechanisms of ATL leukemogenesis following HTLV-1 infection have not been fully elucidated.

The tumor suppressor lung cancer 1 gene (TSLC1) at chromosome 11q23 has been identified as a tumor suppressor gene in non-small-cell lung cancer (9, 13). In contrast, it was recently found to be highly and ectopically expressed in acute-type ATL cells, most ATL cell lines, and HTLV-1-infected T-cell lines (15). Enforced expression of TSLC1 in ATL-derived ED-40515(−) cells resulted in higher aggregations and binding abilities in a human umbilical vein endothelial cell line (HUVEC). These results suggest that TSLC1 might contribute to tumor growth by enhancing aggregation after infiltration and migration outside blood vessels. Since the role of TSLC1 overexpression in the course of tumor growth and organ infiltration of ATL cells remains to be fully elucidated, we investigated the direct involvement of TSLC1 in the growth and infiltration of leukemia cells using C57BL/6J and NOD-SCID/γc^{null} (NOG) mice (4, 8).

In order to analyze the tumorigenicity of TSLC1 expression in leukemia cells, a murine IL-2-independent T-lymphoma cell line (EL4) injected into the intraperitoneum of syngeneic C57BL/6J mice was used as a model for ATL. EL4 cells were transfected with a pcDNA3 expression plasmid containing TSLC1, and transformant cells were selected by a limiting-dilution method in the presence of G-418. We also used EL4 cells expressing a green fluorescent protein-Tax fusion protein (EL4/GAX) (6) and parental EL4 (EL4/p) as a control. Expression of Tax protein in EL4 cells, a 38-kDa band of Tax protein in HUT102 cells, and a 64-kDa band of green fluorescent protein-Tax fusion protein in EL4/GAX cells were all

* Corresponding author. Mailing address for Naoki Yamamoto: AIDS Research Center, National Institute of Infectious Disease, 1-23-1 Toyama, Shinjuku-ku, Tokyo 162-8640, Japan. Phone: 81-3-5285-1111. Fax: 81-3-5285-1165. E-mail: nyama@nih.go.jp. Mailing address for Kazuhiro Morishita: Division of Tumor and Cellular Biochemistry, Department of Medical Sciences, Faculty of Medicine, University of Miyazaki, Kiyotake, Miyazaki, Japan. Phone: 81-9-8585-0985. Fax: 81-9-8585-2401. E-mail: kmorishi@med.miyazaki-u.ac.jp.

† Present address: Department of Pathology, New York University School of Medicine, 550 First Avenue, New York, NY 10016.

▽ Published ahead of print on 15 October 2008.

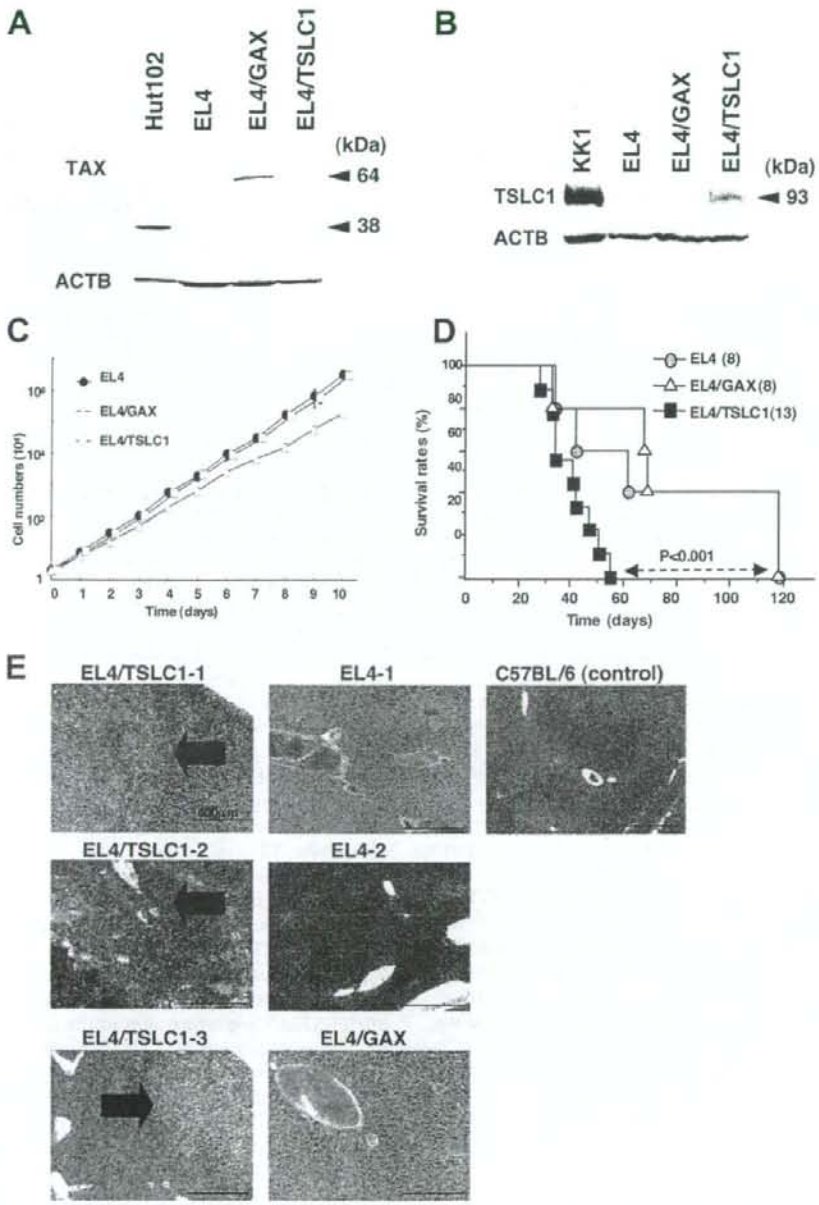

FIG. 1. Transplantation of EL4 T-cell lymphoma cells expressing TSLC1 shortened the life span of syngeneic mice. (A) Expression of Tax protein in HUT102. EL4, EL4/GAX, and EL4/TSLC1 cells was detected by Western blot analysis. Expression of β-actin protein (ACTB) was used as a loading control. (B) Expression of TSLC1 protein in KK1. EL4, EL4/GAX, and EL4/TSLC1 cells was detected by Western blot analysis. Expression of β-actin protein (ACTB) was used as a loading control. (C) Cell numbers in a growth curve are shown for an average of three independent counts, and standard deviations are indicated as error bars. (D) Survival curves of C57BL/6 mice inoculated in the abdominal cavity with EL4, EL4/GAX, or EL4/TSLC1 cells. Cumulative survival rates were calculated by the Kaplan-Meier method and compared using a log-rank test. (E) Liver sections from all mice were stained with hematoxylin-eosin. The regions of liver metastasis (arrow) were seen in liver sections from mice inoculated with EL4/TSLC1 cells but not shown in the liver sections from the mice inoculated with EL4 or EL4/GAX cells. Magnification, ×100; bars, 400 μm.

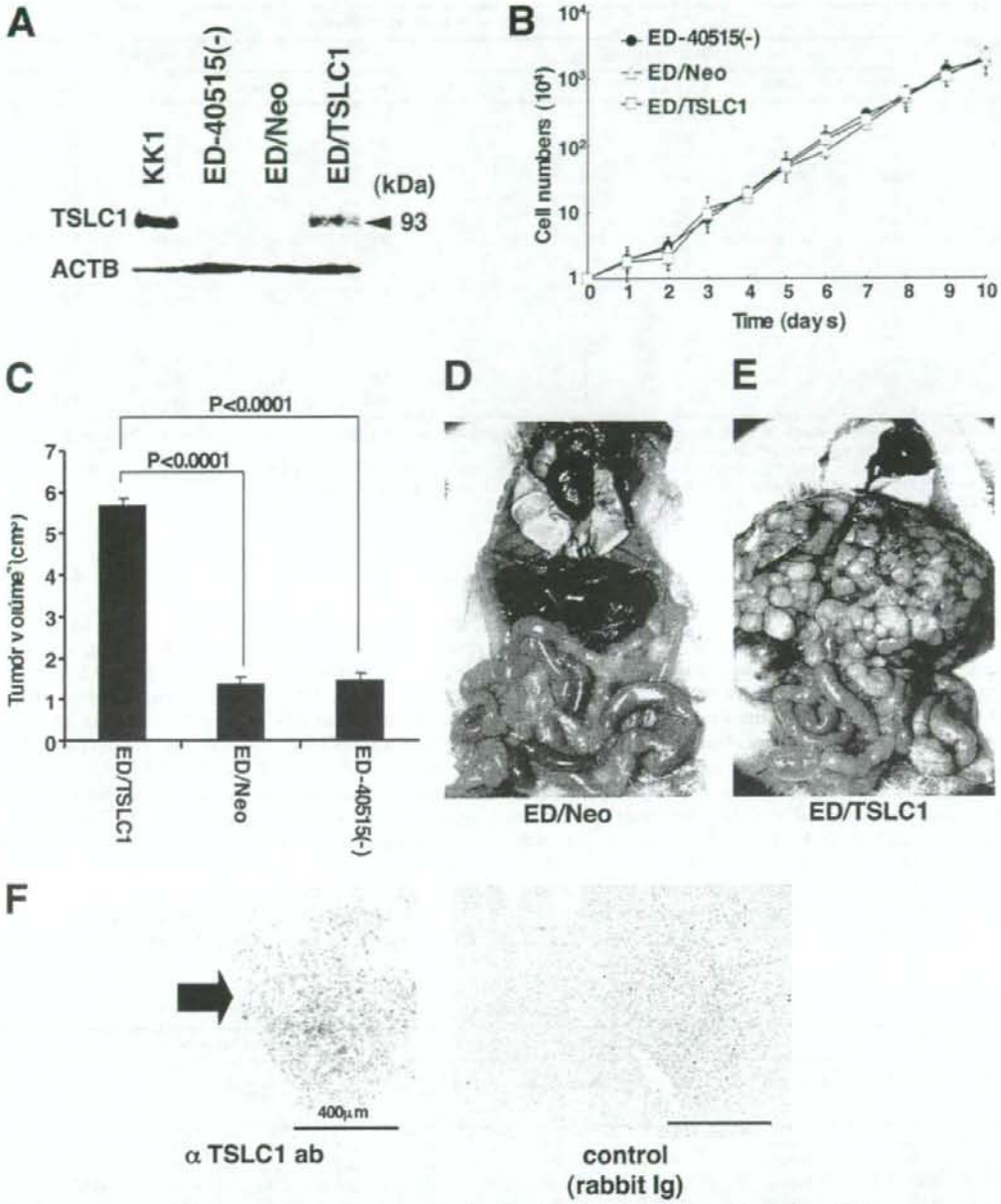

FIG. 2. Involvement of TSLC1 expression in tumor growth and infiltration of leukemia cells in NOG mice. (A) Expression of TSLC1 in KK1, ED-40515(−), ED/Neo, or ED/TSLC1 cell lines was detected by Western blot analysis. Expression of β-actin protein (ACTB) was used as a loading control. (B) Cell growth curves of ED-40515(−), ED/Neo, and ED/TSLC1 cell lines are shown for an average of three independent counts, and standard deviations are indicated as error bars. (C) Tumor volumes of mice inoculated subcutaneously with ED/TSLC1, ED/Neo, or ED-40515(−) cells after 21 days are shown as the means ± standard errors of the means for five mice in each group. Statistical analysis was done with a Student *t* test. (D and E) The pictures shown were derived from gross photographs of the sacrificed mice at 1 month after intravenous inoculation of ED/Neo (D) or ED/TSLC1 (E) cells. (F) Immunohistochemical staining for TSLC1 protein in liver metastases of the mice inoculated intravenously with ED/TSLC1 cells is shown. An arrow indicates a tumor mass with strong staining with a rabbit anti-TSLC1 antibody; however, the same mass shows no staining with rabbit immunoglobulin (Ig) as a negative control. Magnification, ×100; bars, 400 μm.

TABLE 1. Invasion scores of mice inoculated with ED/Neo or ED/TSLC1 cells

Cell line and mouse	Invasion score for organ by observation:									
	Macroscopic[a]					Microscopic[b]				
	Liver	Kidney	Lung	Ovary	Spleen	Liver	Kidney	Lung	Ovary	Spleen
ED/TSLC1										
T1	3+	−	+/−	1+	−	3+	−	2+	2+	−
T2	3+	−	−	1+	−	3+	−	2+	2+	−
T3	3+	−	+/−	2+	−	3+	−	2+	2+	−
T4	3+	−	−	1+	−	3+	−	2+	2+	−
T5	2+	−	−	2+	−	3+	−	2+	3+	−
T6	3+	−	+/−	1+	−	3+	−	+/−	2+	−
ED/Neo										
N1	−	−	−	2+	−	2+	−	+/−	3+	−
N2	+/−	−	−	1+	−	+/−	−	−	2+	−
N3	−	−	−	2+	−	−	−	+/−	2+	−
N4	−	−	−	1+	−	−	−	−	2+	−
N5	−	−	−	1+	−	ND[c]	ND	ND	ND	ND
N6	−	−	−	1+	−	ND	ND	ND	ND	ND

[a] Subjective invasion scores by macroscopic observation were as follows: −, no invasion; +/−, less than 10% invasion in the organ; 1+, 10 to 30% invasion in the organ; 2+, 30 to 70% invasion in the organ; 3+, over 70% invasion in the organ.
[b] Subjective invasion scores by microscopic observation were as follows: −, no invasion; +/−, less than 1% leukemia cells in the section; 1+, less than 10% leukemia cells in the section; 2+, 10 to 30% leukemia cells in the section; 3+, over 30% leukemia cells in the section
[c] ND, not done.

detected by Western blot analysis (Fig. 1A). Expression of a TSLC1 protein in EL4/TSLC1 cells was also shown on Western blot analysis with KK1, an ATL cell line expressing TSLC1 (12) (Fig. 1B). In an in vitro cell growth assay, 2×10^4 cells were incubated, and their growth was analyzed by direct counting with trypan blue dye staining. EL4 and EL4/TSLC1 cells showed nearly identical proliferation profiles in vitro, while Tax-expressing EL4 cells proliferated more slowly (Fig. 1C). This difference in cell growth might be caused by different expression vectors. In an in vivo growth assay, 2×10^6 cells of each cell line were injected into the peritoneal cavity of C57BL/6J mice: eight mice for EL4 cells as controls, 13 mice for EL4/TSLC1 cells, and eight mice for EL4/GAX cells. All of the mice died of tumor invasion of various organs with ascitic fluids in 40 to 120 days. The median survival time of the control mice injected with EL4 cells or EL4/GAX cells was 72 days. The mice with EL4/TSLC1 cells, however, died within 60 days, with a median survival time of 41 days (Fig. 1D). The phenotypes of the control mice and the EL4/TSLC1 mice were almost identical with invasion of tumors into various organs. Organ metastasis of tumor cells in three EL4/TSLC1-inoculated mice, two EL4-inoculated mice, and one EL4/GAX-inoculated mouse was analyzed and evaluated with hematoxylin-eosin staining. The liver was one of the major sites of metastasis in all three of the EL4/TSLC1-inoculated mice by histopathological analysis but not in the two EL4-inoculated mice or the EL4/GAX-inoculated mouse (Fig. 1E). These results support the role of TSLC1 overexpression in T-lymphoma cells as one of an aggressive factor in the development of leukemia/lymphoma.

In order to investigate the possibility that overexpression of TSLC1 promotes tumor growth and/or infiltration in vivo,

TABLE 2. Clinical characteristics of patients and pathological findings of organ invasion[a]

Patient no.	Age (yr)/sex	Clinical characteristic				Invasion score in NOG mice[b]				TSLC1 expression score[c]
		Diagnosis (ATL type)	WBC (10^9/liter)	Lymphocytes (%)	Atypical cells (%)	Liver	Lung	Spleen	Lymph node	
1	73/M	Chronic	7.8	59	47	3+	3+	3+	ND	3+
2	59/F	Chronic	9.0	75	40	3+	2+	2+	1+	2+
3	66/F	Chronic	29.4	49	75	3+	3+	3+	ND	3+
4	44/F	Chronic	22.6	51	45	3+	2+	2+	2+	2+
5	43/F	Chronic	18.6	63	43	3+	3+	3+	ND	2+
6	54/M	Acute	192.8	65	91	1+	2+	ND	ND	1+
7	58/M	Acute	67.3	71	80	3+	3+	3+	ND	2+
8	65/F	Acute	29.4	25	60	3+	2+	ND	3+	3+
9	68/M	Acute	30.0	79	81	3+	1+	1+	2+	2+
10	66/F	Acute	10.2	38	51	3+	3+	3+	ND	3+

[a] Abbreviations: M, male; F, female; WBC, white blood cells; ND, not done.
[b] Subjective invasion scores were as follows: 0, no invasion; 1+, less than 10% leukemia cells in the section; 2+, 10 to 30% leukemia cells in the section; 3+, over 30% leukemia cells in the section.
[c] Subjective scores of TSLC1 expression in pathological immunostaining were as follows: −, no staining; 1+, faint staining in less than 10% of invasive leukemia cells; 2+, weak to moderate staining in 30 to 70% of invasive leukemia cells; 3+, intense staining in more than 70% of invasive leukemia cells.

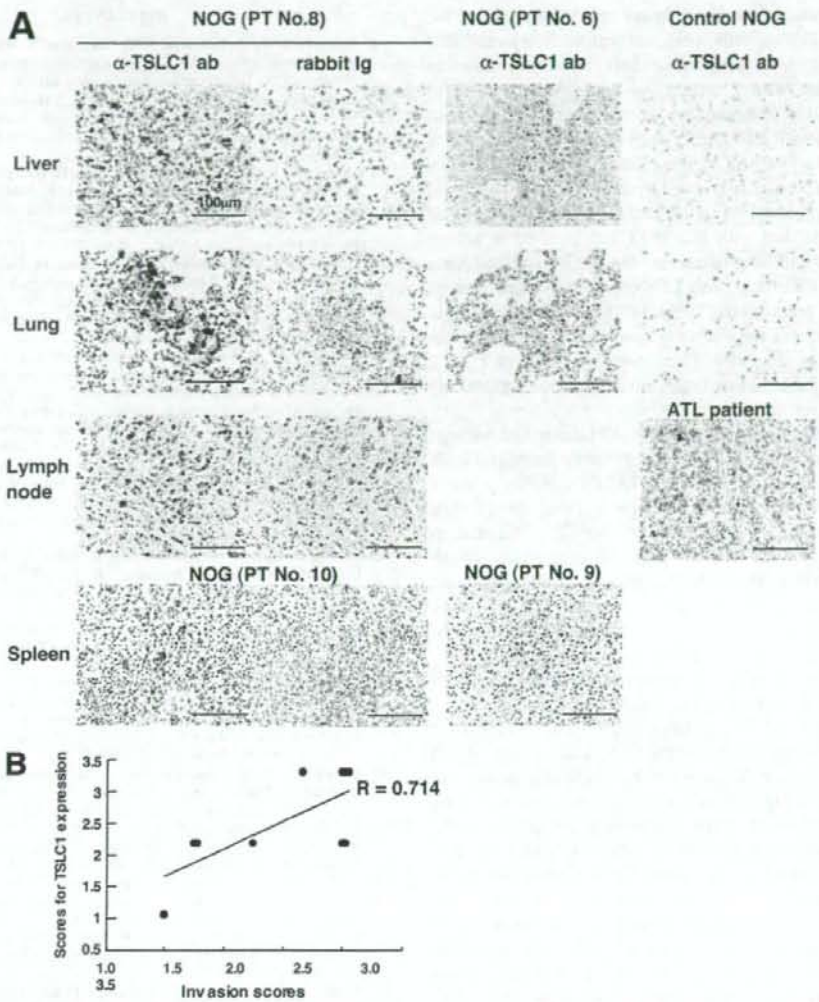

FIG. 3. Growth and infiltration of primary ATL cells in various organs of NOG mice based on TSLC1 expression. (A) Immunohistochemical staining of various organs of NOG mice inoculated with leukemia cells from patient 6, 8, 9, or 10 is shown with the use of rabbit anti-TSLC1 antibody or rabbit immunoglobulin (Ig) as a negative control. Sections from patients 8 and 10 showed severe invasion (invasion score, 3) and dense staining for TSLC1 (expression score, 3), while sections from patients 6 and 9 showed mild invasion (invasion score, 1) and light staining for TSLC1 (expression score, 1). Liver and lung sections from control NOG mice were used as negative controls, and a lymph node from an ATL patient was used as a positive control. Magnification, ×400; bars, 100 μm. (B) The diagram of dispersion between mean values of each invasion score and scores for TSLC1 expression in each NOG mouse inoculated with primary ATL cells showed moderate correlation ($R = 0.714$).

ATL-derived ED-40515(−) cells (10) were injected into NOG mice. Since expression of TSLC1 in ED-40515(−) cells is severely reduced by promoter methylation, they were transfected with either a TSLC1 expression plasmid (pcDNA3/TSLC1) or a mock plasmid (pcDNA3/Neo). ED/TSLC1 and ED/Neo cells were identified by selection with G-418. High levels of TSLC1 expression were verified in the ED/TSLC1 cells, but not in the ED/Neo cells, by Western blot analysis (Fig. 2A). The ED/TSLC1, ED/Neo, and ED-40515(−) cell lines all showed the same proliferation profile in vitro (Fig. 2B). Cells (10×10^6) were inoculated subcutaneously into the postauricular region of NOG mice, which permitted the observation of tumor growth macroscopically and the measurement of tumor size over a relatively short time (3). The ED/TSLC1 cell lines caused greater formation of larger tumors than did the ED/Neo and ED-40515(−) cell lines (Fig. 2C). The development of clinical signs of near-death (e.g., piloerection, weight loss, and cachexia) in mice at the time of killing was also more prevalent with the ED/TSLC1 cell line. These results suggest that TSLC1 expression in ATL cells enhances in vivo tumor growth in NOG mice.

Since the mice died within 4 weeks after subcutaneous in-

oculation of leukemia cells due to heavy tumor burden, 2×10^6 ED/TSLC1 or ED/Neo cells were intravenously injected into six NOG mice in order to investigate their capacity for invasion of various organs. After 1 month, we sacrificed the mice to determine the extent of organ invasion. Macroscopically, all of the mice injected with ED/TSLC1 cells (six/six) showed severe liver invasion with swelling of the ovaries. None of the mice injected with ED/Neo cells showed liver invasion, but they did show ovarian involvement (Fig. 2D and E). Microscopically, all of the mice inoculated with ED/TSLC1 cells showed severe and massive liver and lung invasions. On the other hand, only one of six mice inoculated with ED/Neo cells showed a large amount of liver metastasis (Table 1). TSLC1 expression in tumor cells infiltrating the liver was confirmed by immunohistochemical staining (Fig. 2F). Thus, overexpression of TSLC1 in ATL cells might enhance organ invasion, and particularly invasion of the liver and lung.

Next, we examined whether primary ATL cells with various levels of expression of TSLC1 could efficiently grow and infiltrate various organs in NOG mice. TSLC1-positive primary ATL cells (2×10^7) from five acute-type and five chronic-type ATL patients were inoculated subcutaneously into the postauricular region of NOG mice (Table 2). All of the mice developed clinical signs of near-death (e.g., piloerection, weight loss, and cachexia) 6 to 8 weeks after inoculation, in addition to the enlargement of the lymph nodes, spleen, lungs, and liver. Microscopically, ATL cells invaded various organs of all ATL-bearing NOG mice to different degrees. Based on results of immunohistochemical staining for TSLC1, all invading leukemia cells expressed TSLC1 protein, compared with no TSLC1 expression in these organs in control NOG mice (Table 2 and Fig. 3A). The dispersion diagram for the levels of invasion and the levels of TSLC1 expression in the leukemia cells showed a correlation coefficient of 0.714, suggesting that there was a moderate correlation between invasive capability and the level of TSLC1 expression (Fig. 3B). Thus, TSLC1 could aid in the formation of a rapidly growing large tumor and massive infiltration of ATL cells into various organs in NOG mice. Since TSLC1 is expressed in various types of ATL cells, including smoldering and chronic types, it might be a promising target for the development of a new anti-ATL therapy. The NOG mouse model system described in the present study could provide a novel means by which to understand and investigate the further importance of TSLC1 in ATL progression.

We thank S. Ichinose of the Instrumental Analysis Research Center; S. Endo of the Animal Research Center, Tokyo Medical and Dental University; and Y. Sato of the National Institute of Infectious Diseases for her excellent technical assistance. Anti-Tax (MI73) antibody was the kind gift of Y. Namba and M. Matsuoka (Institute for Virus Research, Kyoto University).

Supported by grants from the Ministry of Education, Science, and Culture; the Ministry of Health, Labor, and Welfare; and Human Health Science of Japan.

REFERENCES

1. **Ballard, D. W., E. Bohnlein, J. W. Lowenthal, Y. Wano, B. R. Franza, and W. C. Greene.** 1988. HTLV-I tax induces cellular proteins that activate the B element in the IL-2 receptor gene. Science **241**:1652–1655.
2. **Cross, S. L., M. B. Feinberg, J. B. Wolf, N. J. Holbrook, F. Wong-Staal, and W. J. Leonard.** 1987. Regulation of the human interleukin-2 receptor chain promoter: activation of a nonfunctional promoter by the transactivator gene of HTLV-I. Cell **49**:47–56.
3. **Dewan, M. Z., K. Terashima, M. Taruishi, H. Hasegawa, M. Ito, Y. Tanaka, N. Mori, T. Sata, Y. Koyanagi, M. Maeda, Y. Kubuki, A. Okayama, M. Fujii, and N. Yamamoto.** 2003. Rapid tumor formation of human T-cell leukemia virus type 1-infected cell lines in novel NOD-SCID/γ_c^{null} mice: suppression by an inhibitor against NF-κB. J. Virol. **77**:5286–5294.
4. **Dewan, M. Z., J. N. Uchihara, K. Terashima, M. Honda, T. Sata, M. Ito, N. Fujii, K. Uozumi, K. Tsukasaki, M. Tomonaga, Y. Kubuki, A. Okuyama, M. Toi, N. Mori, and N. Yamamoto.** 2006. Efficient intervention of growth and infiltration of primary adult T-cell leukemia cells by an HIV protease inhibitor, ritonavir. Blood **107**:716–724.
5. **Felber, B. K., H. Paskalis, C. Kleinman-Ewing, F. Wong-Staal, and G. N. Pavlakis.** 1985. The pX protein of HTLV-I is a transcriptional activator of its long terminal repeats. Science **229**:675–679.
6. **Furuta, R. A., K. Sugiura, S. Kawakita, T. Inada, S. Ikehara, T. Matsuda, and J. Fujisawa.** 2002. Mouse model for the equilibration interaction between the host immune system and human T-cell leukemia virus type 1 gene expression. J. Virol. **76**:2703–2713.
7. **Hinuma, Y., K. Nagata, M. Hanaoka, M. Nakai, T. Matsumoto, K. I. Kinoshita, S. Shirakawa, and I. Miyoshi.** 1981. Adult T-cell leukemia: antigen in an ATL cell line and detection of antibodies to the antigen in human sera. Proc. Natl. Acad. Sci. USA **78**:6476–6480.
8. **Ito, M., H. Hiramatsu, K. Kobayashi, K. Suzue, M. Kawahata, K. Hioki, Y. Ueyama, Y. Koyanagi, K. Sugamura, K. Tsuji, T. Heike, and T. Nakahata.** 2002. NOD/SCID/γcnull mouse: an excellent recipient mouse model for engraftment of human cells. Blood **100**:3175–3182.
9. **Kuramochi, M., H. Fukuhara, T. Nobukuni, T. Kanbe, T. Maruyama, H. P. Ghosh, M. Pletcher, M. Isomura, M. Onizuka, T. Kitamura, T. Sekiya, R. H. Reeves, and Y. Murakami.** 2001. TSLC1 is a tumor suppressor gene in human non-small cell lung cancer. Nat. Genet. **27**:427–730.
10. **Maeda, M., A. Shimizu, K. Ikuta, H. Okamoto, M. Kashihara, T. Uchiyama, T. Honjo, and J. Yodoi.** 1985. Origin of human T-lymphotrophic virus I-positive T cell lines in adult T cell leukemia. Analysis of T cell receptor gene rearrangement. J. Exp. Med. **162**:2169–2174.
11. **Maruyama, M., H. Shibuya, H. Harada, M. Hatakeyama, M. Seiki, T. Fujita, J. Inoue, M. Yoshida, and T. Taniguchi.** 1987. Evidence for aberrant activation of the interleukin-2 autocrine loop by HTLV-1-encoded p40x and T3/Ti complex triggering. Cell **48**:343–350.
12. **Masuda, M., M. Yagita, H. Fukuhara, M. Kuramochi, T. Maruyama, A. Nomoto, and Y. Murakami.** 2002. The tumor suppressor protein TSLC1 is involved in cell-cell adhesion J. Biol. Chem. **277**:31014–31019.
13. **Murakami, Y., T. Nobukuni, K. Tamura, T. Maruyama, T. Sekiya, Y. Arai, H. Gomyou, A. Tanigami, M. Ohki, D. Cabin, P. Frischmeyer, P. Hunt, and R. H. Reeves.** 1998. Localization of tumor suppressor activity important in non-small cell lung carcinoma on chromosome 11q. Proc. Natl. Acad. Sci. USA **95**:8153–8158.
14. **Poiesz, B. J., F. W. Ruscetti, A. F. Gazdar, P. A. Bunn, J. D. Minna, and R. C. Gallo.** 1980. Detection and isolation of type C retrovirus particles from fresh and cultured lymphocytes of a patient with cutaneous T-cell lymphoma. Proc. Natl. Acad. Sci. USA **77**:7415–7419.
15. **Sasaki, H., I. Nishikata, T. Shiraga, E. Akamatsu, T. Fukami, T. Hidaka, Y. Kubuki, A. Okayama, K. Hamada, H. Okabe, Y. Murakami, H. Tsubouchi, and K. Morishita.** 2005. Overexpression of a cell adhesion molecule, TSLC1, as a possible molecular marker for acute type of adult T-cell leukemia. Blood **105**:1204–1213.
16. **Sodroski, J. G., C. A. Rosen, and W. A. Haseltine.** 1984. Transacting transcriptional activation of the long terminal repeat of human T lymphotropic viruses in infected cells. Science **225**:381–385.
17. **Yamaguchi, K., and T. Watanabe.** 2002. Human T lymphotropic virus type-I and adult T-cell leukemia in Japan. Int. J. Hematol. **76**:240–245.
18. **Yoshida, M., I. Miyoshi, and Y. Hinuma.** 1982. Isolation and characterization of retrovirus from cell lines of human adult T-cell leukemia and its implication in the disease. Proc. Natl. Acad. Sci. USA **79**:2031–2035.

Int. J. Cancer: **124,** 622–629 (2009)

An HIV protease inhibitor, ritonavir targets the nuclear factor-kappaB and inhibits the tumor growth and infiltration of EBV-positive lymphoblastoid B cells

Md. Zahidunnabi Dewan[1,2], Mariko Tomita[3], Harutaka Katano[4], Norio Yamamoto[1], Sunjida Ahmed[1], Michiko Yamamoto[5], Tetsutaro Sata[4], Naoki Mori[3]* and Naoki Yamamoto[1,2]*

[1]*Department of Molecular Virology, Graduate School, Tokyo Medical and Dental University, 1-5-45 Yushima, Bunkyo-ku, Tokyo 113-8519, Japan*
[2]*AIDS Research Center, National Institute of Infectious Diseases, 1-23-1 Toyama, Shinjuku-ku, Tokyo 162-8640, Japan*
[3]*Division of Molecular Virology and Oncology, Graduate School of Medicine, University of the Ryukyus, 207 Uehara, Nishihara, Okinawa 903-0215, Japan*
[4]*Department of Pathology, National Institute of Infectious Diseases, 1-23-1 Toyama, Shinjyuku-ku, Tokyo 162-8640, Japan*
[5]*Division of Safety Information on Drug, National Institute of Health Sciences, Food and Chemicals, Setagaya-ku, Tokyo 158-8501, Japan*

Epstein-Barr Virus (EBV)-associated immunoblastic lymphoma occurs in immunocompromised patients such as those with AIDS or transplant recipients after primary EBV infection or reactivation of a preexisting latent EBV infection. In the present study, we evaluated the effect of ritonavir, an HIV protease inhibitor, on EBV-positive lymphoblastoid B cells *in vitro* and in mice model. We found that it induced cell-cycle arrest at G_1-phase and apoptosis through down-regulation of cell-cycle gene cyclin D2 and anti-apoptotic gene survivin. Furthermore, ritonavir suppressed transcriptional activation of NF-κB in these cells. Ritonavir efficiently prevented growth and infiltration of lymphoma cells in various organs of NOD/SCID/γc^{null} mice at the same dose used for treatment of patients with AIDS. Our results indicate that ritonavir targets NF-κB activated in tumor cells and shows anti-tumor effects. These data also suggest that this compound may have promise for treatment or prevention of EBV-associated lymphoproliferative diseases that occur in immunocompromised patients.

Key words: ritonavir; LCLs; NF-κB; NOG mice

Epstein-Barr virus (EBV) is a ubiquitous human γ herpes virus that establishes a latent infection more than 90% of adults worldwide.[1] Immunocompromised individuals such as those with AIDS or transplant recipients are at increased risk for developing aggressive EBV-associated lymphoproliferative diseases. EBV is associated with malignant diseases, including Burkitt's lymphoma,[1,2] nasopharyngeal carcinoma[3,4] and immunoblastic B cell lymphoma of immunosuppressed individuals. Infection of primary B cells with EBV results in transformation with growth of the cells in tight clumps and immortalization of the cells. These immortalized B cells have an immunoblastic morphology and express each of the EBV-encoded small RNAs (EBERs), EBV nuclear antigen (EBNAs) and latent membrane proteins (LMPs).[2,5] EBERs have oncogenic potential through inhibition of PKR.[6] EBNA-2 is a transactivator that up-regulates expression of cellular genes and LMPs. LMP-1 may mediate proliferative and survival effects not only in EBV-transformed B lymphocytes but also in these malignancies that occur long after primary infection. Many immunocompromised patients with EBV-associated immunoblastic lymphoma have tumors at extranodal sites such as the brain, lung, or gastrointestinal tract. The prognosis of EBV-associated lymphomas is very poor for patients with irreversible immunosuppression and treatment options are limited.

Despite the diversity in clinical manifestations of hematopoietic malignancies, strong and constitutive nuclear factor-kappaB (NF-κB) activation was reported to be a unique and common characteristic of malignant cells.[7,8] In resting cells, NF-κB is sequestered as an inactive precursor by association with inhibitory IκBs in the cytoplasm. On stimulation, IκBs are rapidly phosphorylated, ubiquitinated and degraded by a proteasome-dependent pathway allowing active NF-κB to translocate into the nucleus where it can activate the expression of a number of genes.[9] LMP-1 is an oncoprotein that constitutively activates NF-κB to induce B cell proliferation.[7] Lymphoblastoid cell lines (LCLs) express high level of the antiapoptotic proteins BCL-2, BCL-xL, c-IAP1, Bfl-1 and c-FLIP the targets of NF-κB.[10,11] NF-κB activation has been connected with multiple processes of oncogenesis including control of apoptosis, cell-cycle, differentiation and cell migration,[9] and therefore, inhibition of NF-κB was suggested to be a useful strategy for cancer therapy.[12–20] It has been also reported that inhibition of NF-κB in EBV-associated lymphomas results in induction of apoptosis.[21] Therefore, targeting the NF-κB pathway and inhibition of NF-κB activity is a logical strategy for treating EBV-associated lymphomas.

Ritonavir, a human immunodeficiency virus type 1(HIV-1) protease inhibitor, has been successfully used in clinical treatments of HIV infection, with patients exhibiting a marked decrease in HIV viral load and a subsequent increase in $CD4^+$ T-cell counts.[22–25] Evidence of other effects by ritonavir on cellular proteases, such as the cysteine proteases cathepsin D and E, was presented in the drug's original description, albeit at concentrations >500-fold above the concentration required for inhibition of HIV protease.[26] Protease inhibitors have also been shown to directly affect cell metabolism, interfere with host or fungal proteases and block T-cell activation and dendritic-cell function.[27,28] Ritonavir has been shown to inhibit the chymotrypsin-like activity of the 20S proteasome, and it activates the chymotrypsin-like activity of the 26S proteasome conversely.[27,29,30] Ritonavir also has been reported to inhibit the transactivation of NF-κB induced by activators such as TNFα, HIV-1 Tat protein and the human herpesvirus 8 protein ORF74.[31] It is possible that inhibition of NF-κB activation by ritonavir is linked to additional pathways other than inhibition of proteasome.[31] Protease inhibitors also have been shown to have direct antiangiogenic and antitumor activity.[31,32] Recently, we reported that ritonavir inhibits growth and infiltration of ATL cells through targeting NF-κB.[20]

Grant sponsors: Ministry of Education, Science and Culture, The Ministry of Health, Labor and Welfare, Human Health Science of Japan.

Md. Zahidunnabi Dewan's current address is: Department of Pathology, New York University School of Medicine, 550 First Avenue, New York, NY 10016, USA.

Md. Zahidunnabi Dewan and Mariko Tomita contributed equally to this work.

***Correspondence to:** AIDS Research Center, National Institute of Infectious Diseases, 1-23-1 Toyama, Shinjuku-ku, Tokyo 162-8640, Japan. Fax: 8135-285-1165. E-mail: nyama@nih.go.jp (or) Division of Molecular Virology and Oncology, Graduate School of Medicine, University of the Ryukyus, 207 Uehara, Nishihara, Okinawa 903-0215, Japan. Fax: 81-98-895-1410. E-mail: n-mori@med.u-ryukyu.ac.jp.

Received 14 July 2008; Accepted after revision 2 September 2008
DOI 10.1002/ijc.23993
Published online 15 September 2008 in Wiley InterScience (www.interscience.wiley.com).

Publication of the International Union Against Cancer

In the present, we demonstrate that inhibition of NF-κB activity by ritonavir results in marked increase of apoptosis and induce cell-cycle arrest in EBV-positive lymphoblastoid B cells. We found that ritonavir also suppresses the expression of genes involved in antiapoptosis and cell-cycle progression. In addition, we established preclinical models using newly developed NOD/SCID/γc^{null} (NOG) mouse,[16] a unique type of animal, lacking T-, B- and NK-cells to evaluate the efficacy of antitumor and anti-NF-κB therapies. In the murine model, ritonavir at the clinically relevant dose potently inhibited the growth and infiltration of EBV-transformed LCL cells.

Material and methods

Mice and cells

NOG mice were obtained from the Central Institute for Experimental Animals (Kawasaki, Japan). All mice were maintained under specific-pathogen-free conditions in the Animal Center of Tokyo Medical and Dental University (Tokyo, Japan). The Ethical Review Committee of the Institute approved the experimental protocol.

EBV-positive immortalized lymphoblatoid B-cell lines (LCL-Ya, LCL-Ao, LCL-Ka and LCL-Ku) were cultured in RPMI 1640 medium supplemented with 10% heat-inactivated fetal bovine serum (JRH Biosciences, Lenexa, KS), 100 U/ml penicillin, and 10 μg/ml streptomycin. Peripheral blood mononuclear cells (PBMCs) from 3 healthy volunteers were analyzed. Mononuclear cells were isolated by Ficoll-Paque density gradient centrifugation (GE Healthcare Biosciences, Uppsala, Sweden) and washed with PBS.

Cell viability assay

The effect of ritonavir on cell viability of LCLs and PBMCs from healthy donors was examined by the reagent, water-soluble tetrazolium (WST)-8 (Wako Chemicals, Osaka, Japan). Briefly, 2×10^5 cells were incubated in a 96-well microculture plate in the absence or presence of various concentrations of ritonavir. After 72 hr of culture, WST-8 (5 μl) was added for the last 4 hr of incubation and absorbance at 450 nm was measured using an automated microplate reader. Measurement of mitochondrial dehydrogenase cleavage of WST-8 to formazan dye provides an indication of the level of cell viability.

Cell-cycle analysis

Cells were plated at a density of 3×10^5/ml in 60-mm tissue culture dishes. Twelve hours after plating, cells were exposed to 40 μM ritonavir for 24 h. Cell-cycle analysis was performed with the CycleTEST PLUS DNA reagent kit (Becton Dickinson, San Jose, CA). Briefly, cells were washed with a buffer solution containing sodium citrate, sucrose and dimethyl sulfoxide, suspended in a solution containing RNase A, and stained with 125 μg/ml propidium iodide (PI) for 10 min. Cell suspensions were analyzed on EPICS XL flow cytometer (Beckman Coulter, Fullerton, CA) using EXPO32 software. The cell population at each cell-cycle phase was determined with MultiCycle software (Beckman Coulter).

Assay for apoptosis

Cells were plated at a density of 3×10^5/ml in 60-mm tissue culture dishes. Twelve hours after plating, cells were exposed to ritonavir for 72 hr. Apoptosis was quantified by double staining with Annexin-V-Fluos (Roche Diagnostics, Mannheim, Germany) and PI (Backman Coulter) according to the instructions supplied by the manufacturer. Cells were analyzed on EPICS XL flow cytometer (Beckman Coulter) using EXPO32 software.

Western blot analysis

Treated cells were solubilized at 4°C in lysis buffer containing 62.5 mM Tris-HCl (pH 6.8), 2% SDS, 10% glycerol, 6% 2-mercaptoethanol and 0.01% bromophenol blue. Samples were subjected to electrophoresis on SDS-polyacrylamide gels followed by transfer to a polyvinylidine difluoride membrane and probing with the following specific antibodies: polyclonal antibodies against survivin, cyclin D2 (Santa Cruz Biotechnology, Santa Cruz, CA), Bcl-X_L (BD Transduction Laboratories, San Jose, CA) and monoclonal antibodies against Bcl-2, p53, actin (NeoMarkers, Fremont, CA), PARP (BD Transduction Laboratories) and LMP-1 (DAKO, Kyoto, Japan). The protein bands recognized by the antibodies were visualized using the enhanced chemiluminescence system (Amersham, Piscataway, NJ).

Electrophoresis mobility shift assay (EMSA)

Cells were placed in culture at 1×10^6 cells/ml and examined for inhibition of NF-κB 24 hr after exposure to ritonavir. Nuclear proteins were extracted, and NF-κB binding activities to κB element were examined by EMSA as described previously.[8] In brief, 5 μg of nuclear extracts were preincubated in a binding buffer containing 1 μg of poly (dI:dC) (Amersham Biosciences), followed by addition of ^{32}P-labeled oligonucleotide probe containing NF-κB element (5×10^4 c.p.m.). These mixtures were incubated for 15 min at room temperature. The DNA-protein complexes were separated on a 4% polyacrylamide gel and visualized by autoradiography. To examine the specificity of the NF-κB element probe, unlabeled competitor oligonucleotides were preincubated with nuclear extracts for 15 min before incubation with probes. The probe or competitors used were prepared by annealing the sense and antisense synthetic oligonucleotides as follows: a typical NF-κB element from the *IL-2Rα* gene, 5′-gatcCGGCAGGGGAATCTCCCTCTC-3′; and AP-1 element of the *IL-8* gene, 5′-gactGTGATGACTCAGGTT-3′. Underlined sequences represent the NF-κB or AP-1 binding site. To identify NF-κB protein in the DNA protein complex revealed by EMSA, we used antibodies specific for various NF-κB proteins, including p50, p65, c-Rel, RelB and p52 (Santa Cruz Biotechnology), to elicit a supershift DNA protein complex formation. These antibodies were incubated with the nuclear extracts for 45 min at room temperature before incubation with radiolabeled probes.

Inoculation of EBV-positive immortalized LCLs and collection of samples

LCL Cells [LCL-Ya, LCL-Ao, LCL-Ka and LCL-Ku] were washed twice with serum-free RPMI-1640 medium and resuspended in same medium. Mice were anaesthetized with ether and cells were inoculated subcutaneously (sc) in the postauricular region of NOG mice at a dose of 1×10^7 cells per mouse. All mice were sacrificed 3 weeks after inoculation with lymphoma cells. We measured tumor size 3 weeks after inoculation. Tissues and various organs of mice were collected and fixed with Streck Tissue Fixative, then processed to paraffin wax-embedded sections for staining with hematoxylin and eosin (HE) and immunostaining.

PCR primer and conditions

Detection of the BamHI W repeat region of the EBV genome was performed using 100 ng of genomic DNA extracted from LCLs as follows. LCLs were lysed with genomic DNA extraction buffer (100 mM Tris-HCl pH8.0, 5 mM EDTA, 0.2% SDS, 200 mM NaCl and 200 μg/mL proteinase K) and the lysate was incubated at 50°C for 3 hr. After phenol-chloroform extraction, genomic DNA was purified by ethanol precipitation procedure. A 121-bp fragment of the EBV W repeat region was amplified by the forward primer 5′-CGCATAATGGCGGACCTAG-3′ and reverse primer 5′-CAAACAAGCCCACTCCCC-3′ in a 25 μl reaction mixture comprising 1 × AmpliTaq Gold buffer, 3.5 mM MgCl2, 200 μM dNTP, 300 nM primers, 200 nM probe and 0.025 U/μl AmpliTaq Gold. The PCR cycle conditions were as follows: a DNA denaturation and polymerase activation step of 10 min at 95°C and then 40 cycles of amplification (95°C for 15 sec, 60°C for 1 min). PCR products were separated by electrophoresis on agarose gels, stained with ethidium bromide and visualized by UV-light.

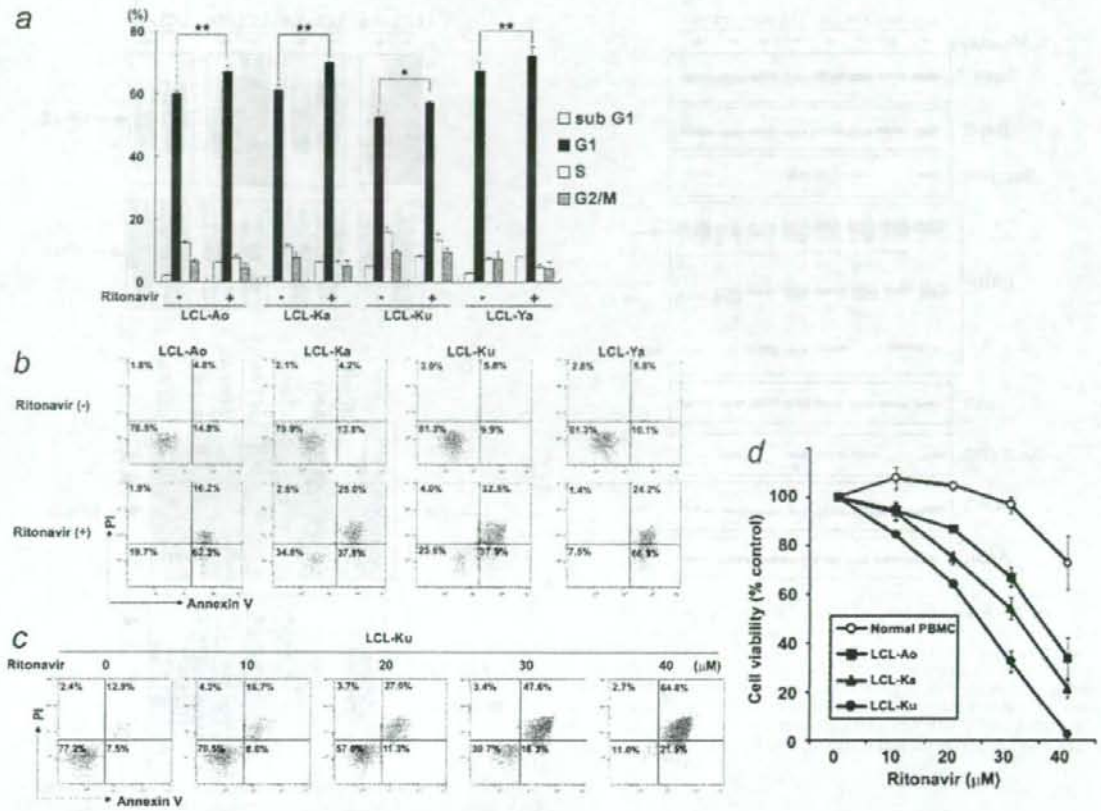

FIGURE 1 – Effect of ritonavir on cell cycle arrest and induction of apoptosis of EBV-positive lymphoblastoid B cells. (*a*) Effect of ritonavir on cell cycle progression of EBV-positive lymphoblastoid B cells. Cells were cultured for 24 hr with (+) or without (−) ritonavir (40 μM). DNA content was analyzed by flow cytometry with PI staining. Sub G_1, S and G_2/M indicate the stages of the cell cycle. Data are expressed as the mean percentages of the cells from three independent experements. Significance of differences between % G_1 of ritonavir treated (+) and untreated (−) cells calculated by Student's *t*-test is shown as *P*-value with astalisk(s). $^*p < 0.05$ and $^{**}p < 0.01$. (*b*) Effect of ritonavir on induction of apoptosis of EBV-immortalized B-cell lines. Cells were cultured for 72 hr with (+) or without (−) ritonavir (40 μM). (*c*) Ritonavir induces apoptosis of EBV-immortalized B-cell lines in a dose-dependent manner. LCL-Ku cells were cultured for 72 hr with increasing concentration of ritonavir (0, 10, 20, 30, 40 μM). Cells were harvested and stained with Annexin-V and PI. Apoptosis was analyzed by flow cytometry. Bottom left quadrants, viable cells; bottom right quadrants, early apoptotic cells. Top right quadrants, nonviable, late apoptotic/necrotic cells. (*d*) Effect of ritonavir on cell viability of LCLs and PBMCs from normal healthy controls. LCLs and PBMCs were incubated in the presence of various concentrations of ritonavir for 72 hr and viability of the cultured cells was measured by WST-8 assay. Relative viability of the cultured cells is presented as the mean determined on LCLs and PBMCs from triplicate cultures. A relative viability of 100% was designated as total number of cells that grew in 72-hr cultures in the absence of ritonavir.

Treatment of tumor-bearing mice with ritonavir

Ritonavir was obtained from Abbott Labs, North Chicago, IL. LCL-Ku cells (1×10^7) were inoculated s.c. in the post-auricular region of NOG mice. The drug was administered s.c. into the tumor cells inoculated site of mice at doses of 30 mg/kg/day, beginning on day 0 for 3 weeks. The control mice received RPMI-1640 (200 μl) simultaneously. In other experiments, ritonavir or RPMI-1640 was also administered intraperitoneally into mice as the same doses stated above, beginning on day 4 for 18 days.

In situ *hybridization*

EBERs were detected by *in situ* hybridization using fluorescein isothiocyanate (FITC)-conjugated EBER PNA (peptide nucleic acid)-probe (DAKO). Briefly, formalin-fixed, paraffin-embedded tissue sections of tumor and various organs were deparaffinized and hydrated in xylenes and graded alcohol series, then rinsed for 5 min in PBS. Deparaffinized samples were incubated with 10 ng/μl of proteinase K for 20 min at 37°C followed by washing, and then incubated with 0.3% methanol for 30 min at room temperature. After washing in PBS, the sections were hybridized with FITC-conjugated EBER-PNA probe in the hybridization solution for 90 min at 56°C. The slides were washed twice in 0.2 × SSC for 20 min at 56°C, and incubated with anti-FITC monoclonal antibody (DAKO) for 45 min at 37°C. Followed by washing, the slides were incubated with horse-radish peroxidase-conjugated polymer reagent (Envision, DAKO) for 30 min at room temperature. Positive staining was visualized after incubation of these samples with a mixture of 0.05% 3.3′-diaminobenzidine tetrahydrochloride in 50 mM Tris-HCl buffer pH7.6 and 0.01% hydrogen peroxide for 5 min. The samples were counterstained with hematoxlin for 2 min, hydrated completely, cleaned in xylene and then mounted. The samples were visualized and photographed under light microscopy (BX41 and DP70; Olympus, Tokyo, Japan).

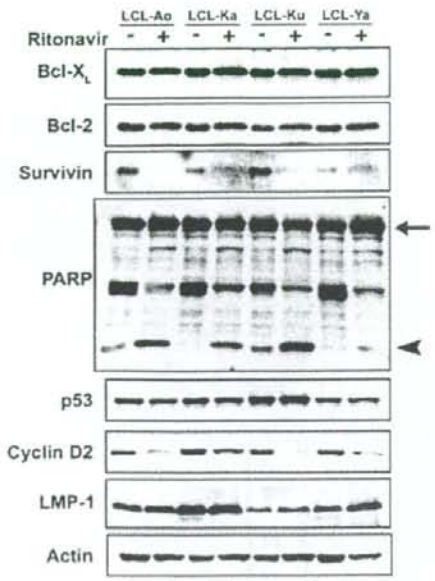

FIGURE 2 – Ritonavir inhibits expression of apoptosis- and cell cycle-associated proteins. EBV-immortalized B-cell lines were cultured with (+) or without (−) ritonavir (40 μM) for 24 hr. Cells were harvested and subjected to Western blot analysis. The polyvinylidene fluoride membrane was sequentially probed with indicated antibodies. Arrow indicates full-length PARP (116 kDa) and arrow head indicates cleaved form of PARP (25 kDa). Essentially the same results were obtained in 3 experiments and representative data are shown.

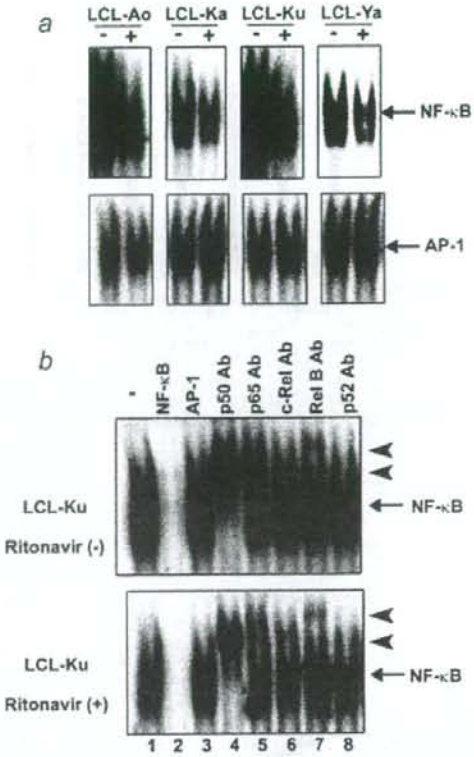

FIGURE 3 – Ritonavir inhibits constitutive NF-κB activation. (*a*) EBV-immortalized B-cell lines were cultured with (+) or without (−) ritonavir (40 μM) for 24 hr and assessed for NF-κB and AP-1-DNA binding activity. (*b*) Cold competition using 100-fold excess of unlabeled NF-κB oligonucleotide, or AP-1 oligonucleotide (lanes 2–3) demonstrated the specificity of the protein/DNA binding complexes. Specificity of NF-κB binding was also determined by using antibodies to the NF-κB components p50, p65, c-Rel, RelB and p52, resulting in supershift (lanes 4–8). Arrows indicate specific complexes of NF-κB with wild type NF-κB oligonucleotide. Arrow heads indicate supershift. Essentially the same results were obtained in 3 experiments and representative data are shown.

Results

Ritonavir induces cell-cycle arrest and apoptosis of LCLs

Ritonavir was examined for its effect on cell-cycle distribution of EBV-immortalized LCLs (Fig. 1*a*). Ritonavir effectively inhibited cell-cycle progression, as evidenced by increased proportion of the cells in G_1 phase of LCL-Ao, LCL-Ka, LCL-Ku and LCL-Ya (LCL-Ao: from 60.1% to 67.1%; LCL-Ka: from 61.2% to 69.9%; LCL-Ku: from 52.6% to 57.3%; and LCL-Ya: from 67.4% to 72.1%). These results indicated that ritonavir induced cell-cycle arrest at G_1-phase. The weak accumulation of cells in G_1 phase by ritonavir suggests that it might rather be an apoptosis inducer than a cell growth inhibitor.

Furthermore, we evaluated the effect of ritonavir on the cell viability of LCLs and PBMCs from healthy individuals (Fig. 1*d*). Ritonavir effectively reduced the survival of LCLs (LCL-Ao, LCL-Ka and LCL-Ku) as measured by WST-8 on the third day of culture in a dose-dependent manner. In contrast, ritonavir hardly affected the survival of PBMCs from healthy volunteers.

The effect of ritonavir on apoptosis was examined by the Annexin-V and PI method. Annexin-V binds to the cells that express phosphatidylserine on the outer layer of the cell membrane, a characteristic feature of cells entering apoptosis. Early apoptotic cells were stained with Annexin V but not with PI. Late apoptotic and necrotic cells were stained with both fluorescent. Ritonavir induced increased proportion of cells positive for Annexin-V and negative for PI in all cell lines (LCL-Ao: from 14.8% to 62.3%; LCL-Ka: from 13.8% to 37.8%; LCL-Ku: from 9.9% to 37.9% and LCL-Ya: from 10.1% to 66.9%) (Fig. 1*b*). Ritonavir also induced dose-dependent increasing of Annexin-V positive and PI negative cells in LCL-Ku cells (Fig. 1*c*), indicating increasing apoptosis of ritonavir-treated cells.

Ritonavir down-regulates the expression of the cell-cycle- and apoptosis-associated genes

The antiproliferative and proapoptotic effects of ritonavir were explored by examining the levels of intracellular regulators of cell-cycle and apoptosis after exposure to ritonavir (Fig. 2). Ritonavir down-regulated the levels of survivin and cyclin D2 in EBV-immortalized B-cell lines. We also observed increased cleavage of PARP in these cells. However, ritonavir did not modulate the other regulators of cell-cycle and apoptosis such as Bcl-X_L, Bcl-2 and p53. Ritonavir had no effect on the expression of viral proteins such as LMP-1, suggesting that ritonavir may induce cell-cycle arrest and apoptosis by down-regulating the levels of survivin and cyclin D2 without reducing the virus levels in the cells.

Ritonavir suppresses constitutive NF-κB expressed by EBV-transformed LCLs

To examine the effect of ritonavir on NF-κB DNA binding, EMSA was performed. EBV-immortalized B-cell lines were incubated with or without 40 μM ritonavir for 24 h, and nuclear extracts were prepared and examined for NF-κB by EMSA.

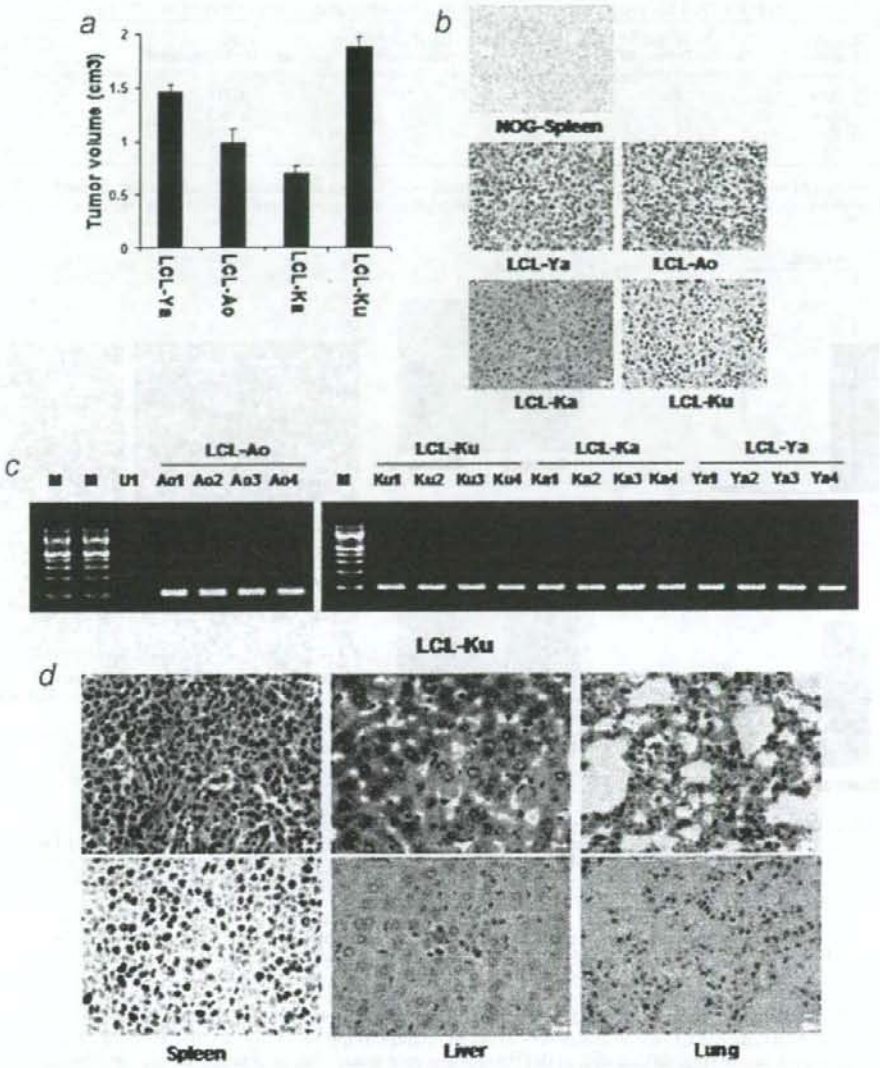

FIGURE 4 – Successful engraftment and infiltration of EBV-positive lymphoblastoid B cells in NOG mice. (*a*) Subcutaneous tumor size in mice 21 days after inoculation with various LCL cells. (*b*) *In situ* hybridization for EBER of spleen from NOG mice not receiving tumor cells, as a negative control and tumor tissues of LCL cells injected mice. Magnification ×40. (*c*) Detection of viral DNA by PCR. M, Marker; U1: EBV-negative U937 cell for negative control; Ao1, *in vitro* culture and Ao2, Ao3 and Ao4, *in vivo* samples from 3 different mice inoculated with LCL-Ao; Ku1, *in vitro* culture and Ku2, Ku3 and Ku4, *in vivo* sample from 3 different mice inoculated with LCL-Ku; Ka1, *in vitro* culture and Ka2, Ka3 and Ka4, *in vivo* sample from 3 different mice inoculated with LCL-Ka, Ya1, *in vitro* culture and Ya2, Ya3 and Ya4, *in vivo* sample from 3 different mice inoculated with. LCL-Ya. Infiltration of EBV-immortalized B-cell lines in various organs of NOG mice. (*d*) HE and *in situ* hybridization for EBER of spleen, liver and lung of mice inoculated with LCL-Ku cells. Left, middle and right panels represent spleen, liver and lung, respectively. Upper and lower panels represent HE and EBER, respectively (magnification ×40).

Down-regulation of NF-κB occurred in all cell lines (Fig. 3*a*, upper panels). Inhibition appeared specific to NF-κB, because no significant change in binding activity of AP-1 was observed after treatment of cells with ritonavir (Fig. 3*a*, lower panels). Also, the observed protein/DNA binding was specific for NF-κB, because the binding was effectively competed and abrogated by excess unlabeled NF-κB oligonucleotide but not by mutant NF-κB or AP-1 oligonucleotide (Fig. 3*b*). LCL-Ku cell extract without ritonavir treatment contained p50, p65 and Rel B proteins in the NF-κB complex (Fig. 3*b*, upper panel), and ritonavir did not affect components of the NF-κB complex (Fig. 3*b*, lower panel).

Efficient engraftment and infiltration of EBV-transformed LCLs in NOG mice

EBV-immortalized LCLs (LCL-Ya, LCL-Ao, LCL-Ka and LCL-Ku) were inoculated s.c. in the post-auricular region of NOG mice (Fig. 4 and Table I). Mice inoculated with LCL cells (LCL-

TABLE I – *IN VIVO* CHARATERISTICS OF EBV-POSITIVE LYMPHOBLASTOID B CELLS IN NOG MICE

Cell line	Orgin/EBV status	No. of cells inoculated/mouse (10^7)[1]	Inoculation route[2]	Day of sacrifice after inoculation	No. of mice with tumor/no. of mice inoculated[3]	Organ-infiltration[4]		
						Spleen	Liver	Lung
LCL-Ya	B/+	1	sc	21	03/03	++	–	–
LCL-Ao	B/+	1	sc	21	03/03	++	–	–
LCL-Ka	B/+	1	sc	21	03/03	++	–	–
LCL-Ku	B/+	1	sc	21	21/21	+++	+	+

[1]Mice were inoculated with 1×10^7 cells per mouse.–[2]sc, subcutaneous.–[3]Number of animals in which tumor developed.–[4]Organ-infiltration was examined by histological analysis.–, no infiltration; +, slight infiltration; ++, marked infiltration; +++, massive infiltration.

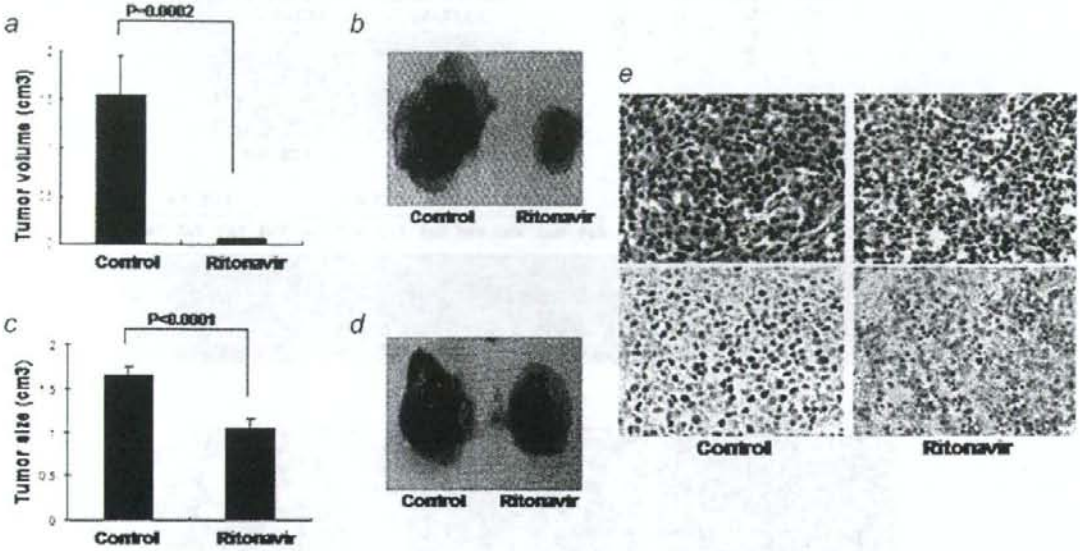

FIGURE 5 – Effect of ritonavir on lymphoma cell growth and infiltration. Mice were injected with LCL-Ku cells (1×10^7 cells) s.c. in the postauricular region. (*a* and *b*) The drug was administered s.c. into the tumor cells inoculated site of mice at doses of 30 mg/kg/day, beginning on day 0 for 3 weeks. The control mice received RPMI-1640 (200 µl) simultaneously. (*a*) Average size of tumor, data represent the mean ± SD from 6 mice. (*b*) Photograph of subcutaneously formed excised tumor without (left) and with (right) ritonavir treatment. (*c* and *d*) Effect of ritonavir on established tumor, ritonavir or RPMI-1640 was also administered intraperitoneally into mice as the same doses stated above, beginning on day 4 for 18 days. (*c*) Average size of tumor, data represent the mean ± SD from 6 mice. (*d*) Photograph of subcutaneously formed excised tumor without (left) and with (right) ritonavir treatment. (*e*) HE and *in situ* hybridization for EBER in spleen tissue of LCL cells injected mice. Magnification ×40. Upper and lower panels show HE and EBER staining, respectively.

Ya, LCL-Ao, LCL-Ka and LCL-Ku) produced a visible tumor within 3 weeks in all NOG mice. LCL-Ku cell was very efficient in the formation of a large tumor (Fig. 4*a*), as well as development of clinical signs of near-death, such as pilorection, weight loss and cachexia in mice at the time point of sacrifice. The average tumor size (LCL-Ya, LCL-Ao, LCL-Ka and LCL-Ku) in NOG mice inoculated s.c. with lymphoma cells was shown in Figure 4*a*. To test whether tumors maintain original histomorphology and expression patterns of tumor markers in NOG, we performed HE and *in situ* hybridization for EBER of normal mice spleen not receiving tumor cells and tumor tissues obtained from mice inoculated with LCLs. Histological analysis revealed that morphologically immunoblastic cells with large nucleus, clear nuclear membrane and broad cytoplasm expressed EBER, whereas EBER was not detected in spleen tissue collected from mice not receiving tumor cells, suggesting that *in vivo* tumor cells preserved well morphology as well as expressed viral gene EBER (Fig. 4*b*). Tumor cells from mice inoculated with EBV-immortalized B-cell lines were positive for DNA of EBV by PCR (Fig. 4*c*). These results showed that EBV-immortalized B-cell lines inoculated s.c. into the postauricular region of NOG mice were able to produce a visible tumor very efficiently. To assess the tissue distribution of lymphoma cells, we carried out histological examinations of the different organs of NOG mice after inoculation of the cells. Proliferation and infiltration of tumor cells were found not only in primary tumor tissues but also in spleen and to a lesser extent in liver and lung of NOG mice inoculated with tumor cells (Table I). HE and *in situ* hybridization staining for EBER showed a degree of infiltration of tumor cells at the site of inoculation and various organs with lymphoma cells (Fig. 4*d*). Interestingly, LCL-Ku cells appeared to infiltrate in various organs of mice more aggressively and massively than other cells. This extremely rapid tumor formation and infiltration in all mice is one of the hallmarks of our clinically relevant animal model without change of histomorphology or tumor marker expression.

Ritonavir suppresses the LCLs growth and infiltration in vivo

To determine the effect of ritonavir on tumor growth and infiltration, we injected LCL-Ku cells (1×10^7) s.c. into the postauricular region of NOG mice. Mice were treated with either RPMI-1640 (as control) or ritonavir (30 mg/kg/day), beginning on either day 0 or day 4. A significant decrease in the size of tumors in mice treated with ritonavir was demonstrated when compared with controls 3 weeks after the injection of tumor cells (Fig. 5*a*). Gross appearance of the mice treated by ritonavir showed apparent

reduction of the tumor mass at 3 weeks after inoculation of tumor cells (Fig. 5*b*). Ritonavir also inhibited the size and growth of established tumors (Fig. 5*c* and 5*d*). Ritonavir at this treatment dosage (30 mg/kg/day for 3 weeks) is well tolerated without adverse findings such as standing of hair, weight loss and cachexia of treated mice, all of which are signs of near death. Clinical evaluation of organ invasion 3 weeks after injection of tumor cells showed that ritonavir treatment inhibited their infiltration into spleen (Fig. 5*e*). In contrast, all control mice showed infiltration with tumor cells into spleen. Organ infiltration of lymphoma cells were analyzed and evaluated by HE and *in situ* hybridization of EBER. Together, these data indicate that ritonavir significantly inhibits lymphoma cell growth and infiltration in various organs of NOG mice (Fig. 5).These results suggest that ritonavir contributes to the reduction of the tumor growth and inhibits the organ infiltration in the mice through targeting the constitutive NF-κB activity.

Discussion

EBV-positive malignancies in immunocompromised patients are associated with high mortality and reduce overall survival period. The various chemotherapies so far developed have not increased significantly the survival of patients with EBV-associated malignancies in immunocompromised patients. Given disappointing results using conventional chemotherapy, new treatment strategies that specially target EBV-transformed cells are need.[1,2] LMP-1 is an oncogene that constitutively activates NF-κB to induce B cell proliferation.[7] It has been previously reported that suppression of high NF-κB activity inhibited cell growth and induced apoptosis of cancer cells as well as EBV-transformed cells both *in vitro* and *in vivo*.[12–20,33] Ritonavir is cytotoxic for different types of malignant cells *in vitro* through affecting proteasomal proteolysis, although concentrations necessary to show the *in vitro* effect exceed the achievable therapeutic drugs level.[27,29,30] It may affect the stabilization of p21, p27 and p53 proteins. Recently, ritonavir has been shown to inhibit NF-κB activity and induce the apoptosis of ATL cells.[20] This led us to investigate whether this drug exhibits anti-tumor effects against EBV-transformed cells *in vitro* and in our preclinical murine model. In the present study, we established a unique murine model that presents aggressive features concerning cell growth and infiltration in SCID mice within 3 weeks. Thus, it represents a novel model to evaluate tissue toxicity and the efficacy of therapeutic agents directed toward the treatment of EBV-associated lymphoproliferative diseases.

The blood-plasma ritonavir concentrations obtained in the therapy of HIV-infection are between 5 to 15 μM,[34] but much higher maximal concentrations (up to 46 μM) have been demonstrated in individual patients.[35] In the present study, we used the concentration of ritonavir for doing *in vitro* experiments from 0 to 40 μM and *in vivo* 30 mg/kg/day used for treatment of AIDS patients. Constitutive and strong NF-κB activation was reported to be a characteristic of LCL and important for LCL growth and survival.[7] Our results indicate that inhibition of NF-κB activity by ritonavir reduced cell growth and induced apoptosis of these cells. This is consistent with down-modulation of NF-κB regulated genes such as antiapoptotic and cell-cycle related genes. Our murine model clearly indicate that 30 mg/kg/day of ritonavir (the same dose used clinically for treating HIV/AIDS patients) significantly inhibits EBV-transformed cell growth and infiltration into various organs of NOG mice. The plasma exposure produced by this dose in mice is only approximately one-half of the plasma exposure observed with the licensed dose of ritonavir in human (600 mg BID). In our murine model, ritonavir at this treatment dosage is well tolerated without severe adverse effects observed in the mice during the treatment period. These data strongly suggest that the HIV protease inhibitor, ritonavir, is a promising antitumor agent against EBV-transformed cells and could be used clinically for treatment of EBV-associated malignancies. These results suggest that anti-tumor activity of ritonavir correlates with suppression of NF-κB activity.

In summary, we have established a novel NOG EBV-associated lymphoma model that presents features similar to patients with EBV-infection in immunocompromised patients. These results also indicate that the HIV protease inhibitor, ritonavir, showed antitumor and anti-NF-κB activity against EBV-transformed cells. Finally, our results strongly suggest that NF-κB serves as a potential molecular target to treat EBV-associated malignancies, and that ritonavir might be used clinically as a single compound or in combination with the reducing dose of chemotherapeutic agents for treatment of patients with life-threatening EBV-associated lymphoproliferative diseases and AIDS-associated lymphomas.

Acknowledgements

We thank D. Kempf and T. Yamada of Abbott Laboratories, S. Ichinose of Instrumental Analysis Research Center and S. Endo of Animal Research Center, Tokyo Medical and Dental University for their advice and assistance with the experiments. We also thank Y. Sato of the National Institute of Infectious Diseases for her excellent technical assistance.

References

1. Rickinson AB, Kieff E. Epstein-Barr virus. In: Fields BN, ed. Fields virology, 4th edn. New York (NY): Lippincott Williams and Wilkins, 2001. Vol. 1, 2575–627.
2. Kieff E, Rickinson AB. Epstein-Barr virus and replication. In: Fields BN, ed. Fields virology, 4th ed. New York (NY): Lippincott Williams and Wilkins, 2001. Vol. 1, 2511–73.
3. Zur Hausen H, Schulte-Holthausen H. Presence of EB virus nucleic acid homology in a "virus-free" line of Burkitt tumour cells. Nature 1970;227:245–48.
4. Nonoyama M, Pagano JS. Homology between Epstein-Barr virus DNA and viral DNA from Burkitt's lymphoma and nasopharyngeal carcinoma determined by DNA-DNA reassociation kinetics. Nature 1973;242:44–7.
5. Rowe M, Lear AL, Croom-Carter D, Davies AH, Rickinson AB. Three pathways of Epstein-Barr virus gene activation from EBNA1-positive latency in B lymphocytes. J Virol 1992;66:122–31.
6. Yamamoto N, Takizawa T, Iwanaga Y, Shimizu N, Yamamoto N. Malignant transformation of B lymphoma cell line BJAB by Epstein-Barr virus-encoded small RNAs. FEBS Lett 2000;484:153–58.
7. Mosialos G, Birkenbach M, Yalamanchili R, VanArsdale T, Ware C, Kieff E. The Epstein-Barr virus transforming protein LMP1 engages signaling proteins for the tumor necrosis factor receptor family. Cell 1995;80:389–99.
8. Mori N, Fujii M, Ikeda S, Yamada Y, Tomonaga M, Ballard DW, Yamamoto N. Constitutive activation of NF-κB in primary adult T-cell leukemia cells. Blood 1999;93:2360–8.
9. Baldwin AS. The NF-κB and IκB proteins: new discoveries and insights. Annu Rev Immunol 1999;14:649–81.
10. Guinness ME, Kenney JL, Reiss M, Lacy J. Bcl-2 antisense oligodeoxynucleotide therapy of Epstein-Barr virus-associated lymphoproliferative disease in severe combined immunodeficient mice. Cancer Res 2000;60:5354–8.
11. Miyake A, Dewan MZ, Ishida T, Watanabe M, Honda M, Sata T, Yamamoto N, Umezawa K, Watanabe T, Horie R. Induction of apoptosis in Epstein-Barr virus-infected B-lymphocytes by the NF-kappaB inhibitor DHMEQ. Microbes Infect 2008;10:748–56.
12. Watanabe M, Dewan MZ, Okamura T, Sasaki M, Itoh K, Higashihara M, Mizoguchi H, Honda M, Sata T, Watanabe T, Yamamoto N, Umezawa K, et al. A novel NF-κB inhibitor DHMEQ selectively targets constitutive NF-κB activity and induces apoptosis of multiple myeloma cells in vitro and in vivo. Int J Cancer 2005;114:32–8.
13. Adams J, Palombella VJ, Elliott PJ. Proteasome inhibition: a new strategy in cancer treatment. Invest New Drugs 2001;18:109–21.
14. Teicher BA, Ara G, Herbst R, Palombella VJ, Adams J. The proteasome inhibitor PS-341 in cancer therapy. Clin Cancer Res 1999; 5:2638–45.

15. Hideshima T, Chauhan D, Richardson P, Mitsiades C, Mitsiades N, Hayashi T, Munshi N, Dang L, Castro A, Palombella V, Adams J, Anderson KC. NF-κB as a therapeutic target in multiple myeloma. J Biol Chem 2002;277:16639–47.
16. Dewan MZ, Terashima K, Taruishi M, Hasegawa H, Ito M, Tanaka Y, Mori N, Sata T, Koyanagi Y, Maeda M, Kubuki Y, Okayama A, et al. Rapid tumor formation of human T-cell leukemia virus type 1-infected cell lines in novel NOD-SCID/γc^{null} mice: suppression by an inhibitor against NF-κB. J Virol 2003;77:5286–94.
17. Kitajima I, Shinohara T, Bilakovics J, Brown DA, Xu X, Nerenberg M. Ablation of transplanted HTLV-I Tax-transformed tumors in mice by antisense inhibition of NF-κB. Science 1992;258:1792–5.
18. Mori N, Yamada Y, Ikeda S, Yamasaki Y, Tsukasaki K, Tanaka Y, Tomonaga M, Yamamoto N, Fujii M. Bay 11–7082 inhibits transcription factor NF-κB and induces apoptosis of HTLV-I-infected T-cell lines and primary adult T-cell leukemia cells. Blood 2002;100:1828–34.
19. Tan C, Waldmann TA. Proteasome inhibitor PS-341, a potential therapeutic agent for adult T-cell leukemia. Cancer Res 2002;62: 1083–6.
20. Dewan MZ, Uchihara JN, Terashima K, Honda M, Sata T, Ito M, Fujii N, Uozumi K, Tsukasaki K, Tomonaga M, Kubuki Y, Okayama A, et al. Efficient intervention of growth and infiltration of primary adult T-cell leukemia cells by an HIV protease inhibitor, ritonavir. Blood 2006;107:716–24.
21. Cahir-McFarland ED, Davidso DM, Schauer SL, Duong J, Kieff E. NF-kappa B inhibition causes spontaneous apoptosis in Epstein-Barr virus-transformed lymphoblastoid cells. Proc Natl Acad Sci USA 2000;97:6055–60.
22. Collier AC. Efficacy of combination antiretroviral therapy. Adv Exp Med Biol 1996;394:355–72.
23. Collier AC, Coombs RW, Schoenfeld DA, Bassett R, Baruch A, Corey L. Combination therapy with zidovudine, didanosine and saquinavir. Antiviral Res 1996;29:99.
24. Collier AC, Coombs RW, Schoenfeld DA, Bassett RL, Timpone J, Baruch A, Jones M, Facey K, Whitacre C, McAuliffe VJ, Friedman HM, Merigan TC, et al. Treatment of human immunodeficiency virus infection with saquinavir, zidovudine, and zalcitabine. AIDS Clinical Trials Group. N Engl J Med 1996;334:1011–17.
25. Markowitz M, Saag M, Powderly WG, Hurley AM, Hsu A, Valdes JM, Henry D, Sattler F, La Marca A, Leonard JM, Ho DD. A preliminary study of ritonavir, an inhibitor of HIV-1 protease, to treat HIV-1 infection. N Engl J Med 1995;333:1534–39.
26. Kempf DJ, Marsh KC, Denissen JF, McDonald E, Vasavanonda S, Flentge CA, Green BE, Fino L, Park CH, Kong XP, Wideburg NE, Saldivar A, et al. ABT-538 is a potent inhibitor of human immunodeficiency virus protease and has high oral bioavailability in humans. Proc Natl Acad Sci USA 1995;92:2484–88.
27. Andre P, Groettrup M, Klenerman P, de Giuli R, Booth BL, Jr, Cerundolo V, Bonneville M, Jotereau F, Zinkernagel RM, Lotteau V. An inhibitor of HIV-1 protease modulates proteasome activity, antigen presentation, and T cell responses. Proc Natl Acad Sci USA 1998; 95:13120–24.
28. Liang JS, Distler O, Cooper DA, Jamil H, Deckelbaum RJ, Ginsberg HN, Sturley SL. HIV protease inhibitors protect apolipoprotein B from degradation by the proteasome: a potential mechanism for protease inhibitor-induced hyperlipidemia. Nat Med 2001;7:1327–31.
29. Schmidtke G, Holzhütter HG, Bogyo M, Kairies N, Groll M, de Giuli R, Emch S, Groettrup M. How an inhibitor of the HIV-I protease modulates proteasome activity. J Biol Chem 1999;274:35734–40.
30. Gaedicke S, Firat-Geier E, Constantiniu O, Lucchiari-Hartz M, Freudenberg M, Galanos C, Niedermann G. Antitumor effect of the human immunodeficiency virus protease inhibitor ritonavir: induction of tumor-cell apoptosis associated with perturbation of proteasomal proteolysis. Cancer Res 2002;62:6901–8.
31. Pati S, Pelser CB, Dufraine J, Bryant JL, Reitz JMS, Weichold FF. Antitumorigenic effects of HIV protease inhibitor ritonavir: inhibition of Kaposi sarcoma. Blood 2002;99:3771–9.
32. Sgadari C, Barillari G, Toschi E, Carlei D, Bacigalupo I, Baccarini S, Palladino C, Leone P, Bugarini R, Malavasi L, Cafaro A, Falchi M, et al. HIV protease inhibitors are potent anti-angiogenic molecules and promote regression of Kaposi sarcoma. Nat Med 2002;8:225–32.
33. Katano H, Pesnicak H, Cohen JI. Simvastatin induces apoptosis of Epstein-Barr virus (EBV)-transformed lymphoblastoid cell lines and delays development of EBV lymphomas. Proc Natl Acad Sci USA 2004;101:4960–5.
34. Norvir, Ritonavir Product monograph. North Chicago, IL: Abbott laboratories, 1997.
35. Gatti G, Di Biagio A, Casazza R, De Pascalis C, Bassetti M, Cruciani M, Vella S, Bassetti D. The relationship between ritonavir plasma levels and side-effects: implications for therapeutic drug monitoring. AIDS 1999;13:2083–9.

研究成果の刊行に関する一覧表
平成 20 年度　慶應義塾大学医学部　熱帯医学・寄生虫学教室　竹内　勤

雑誌

発表者氏名	論文タイトル名	発表誌名	巻号	ページ	出版年
Takuya Maeda, Tomoya Saito, Omar S. Harb, David S. Roos, Satoru Takeo, Hiroko Suzuki, Takafumi Tsuboi, Tsutomu Takeuchi, Takashi Asai	Pyruvate Kinase type-II isozyme in Plasmodium falciparum localizes to the apicoplast	Parasitology International	58	101-105	2009
Jun Suzuki, Seiki Kobayashi, Ph.D., Rie Murata, Hideo Tajima, D.V.M., Fumitaka Hashizaki, D.V.M., Yoshitoki Yanagawa, D.V.M., Ph.D., Tsutomu Takeuchi, M.D., Ph.D.	A SURVEY OF AMOEBIC INFECTIONS AND DIFFERENTIATION OF AN ENTAMOEBA HISTOLYTICA-LIKE VARIANT(JSK2004) IN NONHUMAN PRIMATES BY A MULTIPLEX POLYMERASE CHAIN REACTION	Journal of Zoo and Wildlife Medicine	39	370-379	2008
Masashi Ohtani, Shigenori Nagai, Shuhei Kondo, Shinta Mizuno, Kozue Nakamura, Masanobu Tanabe, Tsutomu Takeuchi, Satoshi Matsuda, Shigeo Koyasu	Mammalian target of rapamycin and glycogen synthase kinase 3 differentially regulate lipopolysaccharide-induced interleukin-12 production in dendritic cells	IMMUNO-BIOLOGY	112	635-643	2008
Tomoya Saito, Manami Nishi, Muoy l. Lim, Bo Wu, Takuya Maeda, Hisayuki Hashimoto, Tsutomu Takeuchi, David S. Roos, Takashi Asai	A Novel GDP-dependent Pyruvate Kinase Isozyme from Toxoplasma gondii Localizes to Both the Apicoplast and the Mitochondrion	THE JOURNAL OF BIOLOGICAL CHEMISTRY	283	14041-14052	2008
Jun Suzuki, Seiki Kobayashi, Ise Iku, Rie Murata, Yoshitoki Yanagawa and Tsutomu Takeuchi	Seroprevalence of Entamoeba histolytica Infection in Female Outpatients at a Sexually Transmitted Disease Sentinel Clinic in Tokyo, Japan	Jpn. J. Infect. Dis.	61	175-178	2008
Kazutomo Suzue, Seiki Kobayashi, Tsutomu Takeuchi, Mamoru Suzuki Shigeo Koyasu	Critical role of dendritic cells in determining the T_h1/T_h2 balance upon Leishmania major infection	International Immunology	20	337-343	2008

Parasitology International 58 (2009) 101–105

Contents lists available at ScienceDirect

Parasitology International

journal homepage: www.elsevier.com/locate/parint

Short communication

Pyruvate kinase type-II isozyme in *Plasmodium falciparum* localizes to the apicoplast

Takuya Maeda [a,1], Tomoya Saito [a], Omar S. Harb [b], David S. Roos [b], Satoru Takeo [c], Hiroko Suzuki [c], Takafumi Tsuboi [c], Tsutomu Takeuchi [a], Takashi Asai [a,*]

[a] Department of Tropical Medicine and Parasitology, School of Medicine, Keio University, 35 Shinanomachi, Shinjuku-ku, Tokyo 160-8582, Japan
[b] Department of Biology, University of Pennsylvania, 301 Goddard Laboratories Philadelphia, PA 19104, USA
[c] Cell-Free Science and Technology Research Center, Ehime University, 3 Bunkyo-cho, Matsuyama, Ehime 790-8577, Japan

ARTICLE INFO

Article history:
Received 16 July 2008
Received in revised form 15 October 2008
Accepted 18 October 2008
Available online 31 October 2008

Keywords:
Plasmodium falciparum
Pyruvate kinase II
Apicoplast
Mitochondria
Cell-free expression

ABSTRACT

Bioinformatics research on *Plasmodium falciparum* revealed two isoforms of pyruvate kinase: type-I and type-II enzymes. The type-I enzyme shows typical glycolytic properties, while type-II enzyme is involved in fatty acid type-II biosynthesis and has been predicted to localize to the apicoplast with the targeting signal in its N-terminus. The type-I and type-II isoforms have the same evolutionary origin as *Toxoplasma gondii* isozymes, *Tg*PyKI and *Tg*PyKII, respectively; however, *Tg*PyKII localizes to both the mitochondrion and the apicoplast. Accordingly, we made a recombinant full length of *P. falciparum* pyruvate kinase type-II protein using a wheat germ cell-free expression system and obtained a specific antibody against the type-II protein. Fluorescent microscopic analysis revealed that *P. falciparum* type-II enzyme was localized only to the apicoplast, not to the mitochondrion. The data suggest differences in localization and metabolic pathways between *P. falciparum* and *T. gondii* pyruvate kinase isoforms.

Pyruvate kinase (EC 2.7.1.40) catalyzes the essentially irreversible transphosphorylation of phosphoenolpyruvate (PEP) to ADP. The activities of most mammalian and bacterial pyruvate kinases are allosterically regulated by fructose 1,6-bisphosphate, and pyruvate kinase is known to play a regulatory role in glycolysis. The glycolytic end product, pyruvate, feeds into various metabolic pathways, and hence pyruvate kinase is important in several primary metabolic reactions.

Many organisms have pyruvate kinase isozymes with different kinetic properties, and most pyruvate kinases in eukaryotes are reported to be located in the cytosol. Two types of pyruvate kinase were characterized in *Toxoplasma gondii* [1,2]. Pyruvate kinase type-II isozyme (*Tg*PyKII) was localized in both the mitochondrion and the apicoplast, whereas pyruvate kinase type-I (*Tg*PyKI) was located in the cytosol. *Tg*PyKII exhibited only 18% overall amino acid identity with *Tg*PyKI and showed novel properties of exhibiting high pH optima and GDP dependency [2].

The malaria bioinformatics website (http://sites.huji.ac.il/malaria/), compiled and maintained by Hagai Ginsburg, reports two isoforms of pyruvate kinase in *Plasmodium falciparum*. The type-I enzyme (*Pf*PyKI) has been characterized enzymologically in detail [3]. The type-II enzyme (*Pf*PyKII) was predicted to have an apicoplast targeting signal in the N-terminus; however, experimental localization has not been confirmed. Phylogenetic analysis indicated that *Pf*PyKI and *Pf*PyKII have the same evolutionary origin as *Tg*PyKI and *Tg*PyKII, respectively, suggesting that type-II has a proteobacterial origin [2]. Thus, we questioned whether both *Pf*PyKII and *Tg*PyKII are localized in both the apicoplasts and the mitochondria.

In this study, we made recombinant *Pf*PyKII protein in a wheat germ cell-free expression system, purified the recombinant protein, created an antibody, and localized *Pf*PyKII by immunofluorescent microscopy.

The *Pf*PyKII gene was amplified from *P. falciparum* genomic DNA. The two primers were 5′-ACTGGATCCCCATATTGCCTATGAT-3′ and 5′-TCGGGATCC CTAATTTGTTAGACATGG-3′ (*Bam*HI site is underlined). The first denaturation at 95 °C was for 10 min and each of 30 reaction cycles consisted of 94 °C for 30 s, 47 °C for 30 s, and 65 °C for 2 min, and a final elongation cycle step at 65 °C for 5 min using KOD-plus DNA polymerase (Toyobo Co. Ltd, Osaka, Japan). Thereafter, the amplified DNA products were treated with *Bam*HI and inserted into a plasmid pEU-E01G-N2 (Cell-Free Science and Technology Research Center, Ehime University, Ehime, Japan) using the LigaFast ligation kit (Promega, Madison, WI, USA) according to the manufacturer's protocol. The plasmid was electroporated into the *Escherichia coli* DH10B (Takara Bio, Kyoto, Japan) and the bacteria were grown in a plate. The right directional clones were detected by DNA sequencing using the ABI PRISM BigDye terminator cycle sequencing kit (Applied Biosystems, Foster, CA, USA) and loaded onto an ABI PRISM 310 DNA sequencer. After plasmid purification

* Corresponding author. Tel.: +81 3 3353 1211x62747; fax: +81 3 3353 5958.
E-mail address: asait@sc.itc.keio.ac.jp (T. Asai).
[1] Present address: International Research Center for Infectious Diseases, The Institute of Medical Science, The University of Tokyo, Shiroganedai 4-6-1, Minato-ku, Tokyo 108-8639, Japan.

1383-5769/$ – see front matter © 2008 Elsevier Ireland Ltd. All rights reserved.
doi:10.1016/j.parint.2008.10.005

using Qiagen Plasmid Midi Kit (Qiagen, Hilden, Germany), the plasmid was further purified by C_5Cl_2 ultra-centrifugation at 391,000 ×g for 16 h at 25 °C to avoid endotoxin contamination. The purified plasmid containing a glutathione S-transferase (GST) coding region and an SP6 promoter upstream of the DNA inserted region was treated with SP6 RNA polymerase (GE Healthcare, Little Chalfont, Buckinghamshire, UK). The method of mRNA production and translation in wheat germ was described previously [4].

The GST-pyruvate kinase isozyme fusion protein in the wheat germ extract was purified using an affinity column of glutathione sepharose 4B (GE Healthcare). The pyruvate kinase isozyme was cut from the fusion protein by PreScission Protease (GE Healthcare) according to

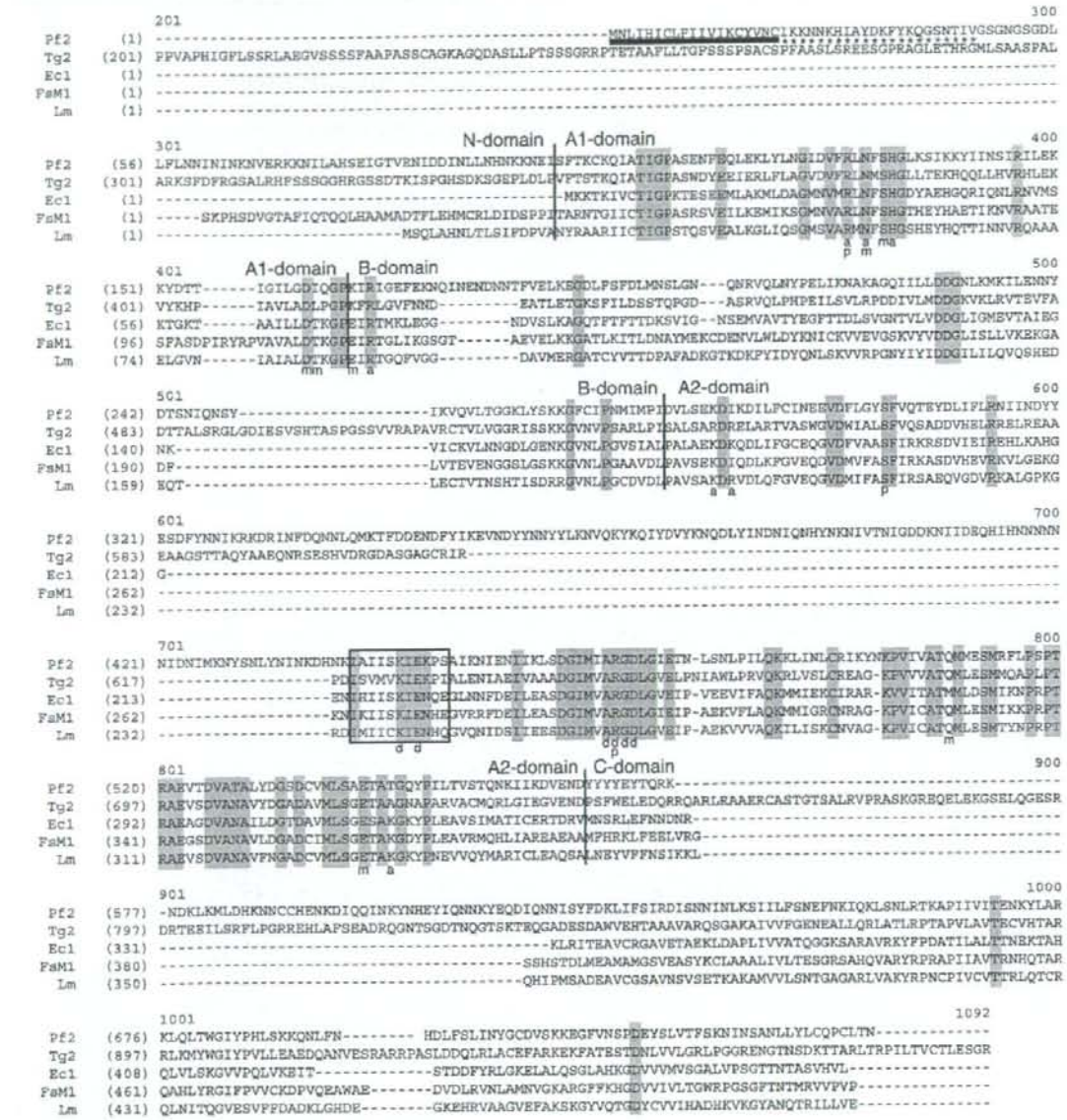

Fig. 1. Amino acid sequence alignment of *P. falciparum* pyruvate kinase type-II isozyme (*Pf*PyKII) with four pyruvate kinases from other species. Sequence data accession numbers are: Pf2, *Pf*PyKII (this study; PF10_0363); Tg2, *Toxoplasma gondii* II (AB118155); Ec1, *Escherichia coli* isozyme I (1PKY_A); FsM1, *Felis catus* isozyme M1 (P11979); Lm, *Leishmania mexicana* (CAA52898). *Vertical lines* indicate divisions between four three-dimensional domains (N, A, B, and C) as described previously [10]. An open black box indicates the pyruvate kinase signature sequence (PROSITE, PS00110); *p* indicates PEP binding sites; *a*, ADP binding sites; *d*, divalent cation binding sites; *m*, monovalent cation binding sites; *dashes*, gaps in the alignment. DNA sequences analyses were performed using the VectorNTI suite (InforMax, Executive Way Frederick, MD, USA). The thick underline in the N-terminal of *P. falciparum* sequence is signal sequence, and following asterisks indicates probable plastid transit peptide. It is conceivable that these sequences compose apicoplast targeting signal. Targeting signals in the N-terminal were analyzed by SignalP [11] and PlasmoAP [12].

the manufacturer's recommendations. Pyruvate kinase isozyme purity was analyzed by SDS–PAGE on 8% polyacrylamide gel as described by Laemmli [5] (Data not shown). The recombinant protein concentration was determined by Bradford assay [6] using bovine serum albumin (BSA) as a standard.

Anti-recombinant *Pf*PyKII antibody was produced through a commercial company (Immuno-Biological Laboratories, Takasaki, Japan). Briefly, purified recombinant *Pf*PyKII from wheat germ extracts was used to immunize a BALB/c mouse. Following six injections of pyruvate kinase isozyme (5 μg each) at 1-week intervals, the whole IgG was isolated from peritoneal fluid with a HiTrap rProtein A FF column (GE Healthcare). The whole cell lysate of 1×10^8 erythrocytic stage *P. falciparum* parasites (FCR-3 strain) was separated on 8% acrylamide gel and blotted onto a nitrocellulose Hybond-C Extra membrane (GE Healthcare). The membrane was blocked for 20 min with 2% skimmed milk in Tris-buffered saline containing 0.2% Tween 20, incubated for 1 h with primary antibodies (1:3000), probed with alkaline phosphatase-conjugated goat anti-mouse IgG (Vector Laboratories, Burlingame, CA, USA) (1:5000), and detected with a BCIP-NBT system (Roche, Basel, Switzerland). Molecular sizes of the protein bands were determined with reference to pre-stained Rainbow molecular weight markers (GE Healthcare).

Cells were fixed and stained using the procedures described by Tonkin et al. [7]. Cells were briefly fixed with 4% EM grade paraformaldehyde (ProSciTech, Thuringowa, Queensland, Australia) and 0.0075% EM grade glutaraldehyde (ProSciTech) in phosphate-buffered saline (PBS) for 30 min. Fixed cells were washed once in PBS and permeated with 0.1% Triton X-100/PBS for 10 min. Cells were washed again and treated with 0.1 mg/ml of sodium borohydride ($NaBH_4$)/PBS for 10 min. Following another wash, cells were blocked in 3% BSA/PBS for 1 h. For staining anti-*Pf*PyKII antibody-binding structure and apicoplast, anti-*Pf*PyKII mouse antibody (diluted 1/1000) and anti-acyl carrier protein (ACP) rabbit antibody (diluted 1/500; gifted by Geoff McFadden, University of Melbourne, Australia) were added and allowed to bind for a minimum of 1 h in 3% BSA/PBS. AlexaFluor goat anti-mouse 594 (red) and anti-rabbit 488 (green) secondary antibodies (Invitrogen, Carlsbad, CA, USA) were added at 1:1000 dilution (in 3% BSA/PBS) and allowed to bind for 1 h, while cells settled onto a previously flamed cover slip coated with 1% polyethylenimine (PEI; Sigma, St Louis, MO, USA). For staining the anti-*Pf*PyKII antibody-binding structure and mitochondrion, citrate synthase-GFP construct (gifted by Geoff McFadden) transformed *P. falciparum* was used. Anti-*Pf*PyKII mouse antibody (diluted 1/1000) was added and allowed to bind for 1 h, followed by addition of AlexaFluor goat anti-mouse 488 (green) antibody and Cy5-conjugated anti-GFP rabbit (red) antibody (diluted 1/1000; Sigma) and allowed to bind for 1 h. Cells were mounted in 50% glycerol with 0.1 mg/ml of 1,4-diazabicyclo[2,2,2]octane (DABCO, Sigma). The microscopic system was a DeltaVision restoration system (Applied Precision, Washington, USA) on an Olympus IX70 inverted microscope equipped with a mercury vapor lamp (100 W) and appropriate barrier emission filters. Images were taken 0.2 μm apart and deconvolved using softWoRx Explorer Suite (Applied Precision).

The deduced amino acid sequence of *Pf*PyKII (NCBI Accession# NP_700836), exhibiting low overall identity (21%) to that of *Pf*PyKI (NCBI Accession# CAG25081), contained a pyruvate kinase signature (PROSITE; PS00110) as did other species and other consensus regions, such as multiple binding sites of ADP, PEP, and divalent cations (Fig. 1). Based on protein alignment, *Pf*PyKII was predicted to be a monovalent cation-independent enzyme. Most of the monovalent cation-binding sites were conserved; however, two binding sites, Thr^{113} and Glu^{117} (in *Felis catus* pyruvate kinase), were substituted by Ile and Lys, respectively. These substitutions are a common characteristic of monovalent cation-independent pyruvate kinases. We found three-specific long insertions in the middle of domain B, A2, and C of *Pf*PyKII, as in *Tg*PyKII. These insertions were different in length, but the insert positions were the same as in *Tg*PyKII.

Following six injections of pyruvate kinase isozyme at 1-week intervals, the whole IgG was isolated from mouse peritoneal fluid. Western blot analysis showed a single band (~80 kDa) in the *P. falciparum* lysate (Fig. 2), which was different from the mass in the type-I enzyme (55.6 kDa), indicating no cross-reaction with the type-I enzyme. Preimmune serum detected no bands in the 1×10^8 *P. falciparum* lysate (data not shown). The antibody was used in immunofluorescence microscopy.

The stained structure from the anti-*Pf*PyKII antibody in *P. falciparum* merged into the apicoplast stained pattern (Fig. 3A), suggesting that *Pf*PyKII localizes to the apicoplast. To determine if *Pf*PyKII localizes to the mitochondria, we analysed the immunolocalization of *Pf*PyKII in a *P. falciparum* cell line expressing the citrate synthase fused to GFP, which targets to the mitochondria [7] (Fig. 3B). The merged image showed that anti-*Pf*PyKII stain is adjacent to, but not associated with, the mitochondria. The two stains were distinguishable in all the stages (data not shown). Thus, we concluded that *Pf*PyKII localizes to the apicoplast, not to the mitochondrion. The data indicate a different localization of type-II pyruvate kinase in *P. falciparum* from that in *T. gondii*.

A recombinant protein of *P. falciparum* pyruvate kinase type-II isozyme (*Pf*PyKII) was created using a wheat germ cell-free system. All our previous attempts for production of this recombinant protein in *E. coli* systems have failed. Probably, it was due to its biased codon usage. The efficiency of production of the protein in our study was not high; nevertheless, the wheat germ cell-free system is useful for creation of the recombinant protein.

In addition, we showed localization of *Pf*PyKII in the apicoplast by immunofluorescent assay. Despite its proteobacterial origin, *Pf*PyKII was localized only to the apicoplast, not to the mitochondrion as in *Tg*PyKII, which is localized to both the mitochondrion and the apicoplast. The difference in metabolic pathways in the organelles between *T. gondii* and *P. falciparum* might reflect differences in their internal environment and in the metabolic relationships between those organelles in the two parasites. Further investigation to reveal these potential differences will contribute to understanding survival of *T. gondii* and *P. falciparum* in the host.

As suggested by Ralph et al. [8], pyruvate kinase in the apicoplast might dephosphorylate PEP imported into the apicoplast via PEP transporter on the apicoplast membrane and supply pyruvate for fatty acid synthesis and the non-mevalonate 1-deoxy-D-xylulose-5-phophate (DOXP) pathway in the organelle. Fleige et al. [9], reporting on carbohydrate metabolism in the *T. gondii* apicoplast, indicated that *Tg*PykII was localized in the apicoplast. These findings suggest differences between *T. gondii* and *P. falciparum* in the mitochondrion and apicoplast metabolic pathways, even though *T. gondii*

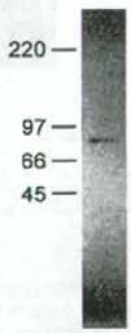

Fig. 2. Specificity of anti-*Pf*PyKII IgG shown by Western blot analysis. The purified recombinant *Pf*PyKII was detected by Western blot analysis with the antibody against the recombinant *Pf*PyKII. Rainbow molecular weight markers (kDa) are indicated on the left.